Chemical Engineering Journal 519 (2025) 164504

Contents lists available at ScienceDirect

Chemical Engineering Journal

journal homepage: www.elsevier.com/locate/cej

Removal of (Brominated) flame retardants in the dissolution recycling of polystyrene

Michiel Van Melkebeke [a], Rita Kol [a], Amin Shariatmadar Tehrani [a], Dave Manhaeghe [a], Emile Casiries [a], Tine Van Laere [a], Yufei Xie [b], Hamed Mohamadzadeh Shirazi [b], Norbert Niessner [c], Dirk Reichert [d], Hilde Poelman [b], Kevin Van Geem [b], Steven De Meester [a,*]

[a] Laboratory for Circular Process Engineering (LCPE), Department of Green Chemistry and Technology, Ghent University, Graaf Karel de Goedelaan 5, Kortrijk 8500, Belgium
[b] Laboratory for Chemical Technology (LCT), Department of Materials, Textiles and Chemical Engineering, Ghent University, Technologiepark Zwijnaarde 125, Zwijnaarde B-9052, Belgium
[c] INEOS Styrolution GmbH, Mainzer Landstraße 50, Frankfurt am Main 60325, Germany
[d] DESOTEC NV, Regenbeekstraat 44, Roeselare 8800, Belgium

ARTICLE INFO

Keywords:
Dissolution recycling
WEEE plastic
Flame retardants
Adsorption
Filtration
COSMO-RS

ABSTRACT

End-use plastic applications can contain potentially harmful additives such as brominated flame retardants (FRs) that complicate their recycling process. Therefore, effective removal of such substances becomes essential to widen the applicability of the recycling process and increase the quality of the recyclate. To that end, this work proposes a combination of filtration and adsorption as purification technique in the dissolution recycling of polystyrene (PS). Five FRs were selected (i.e., HBCD, TBBPA, DBDPE, TPHP, and PolyFR) with two different solvents (i.e., n-butyl acetate and cyclohexene). Based on their solubility, determined both experimentally and through COSMO-RS modeling, the removal of the FRs was investigated by either filtration or adsorption. Results indicate a near complete removal of undissolved FRs via filtration (i.e., >99 wt%), while for the dissolved FRs an optimal removal efficiency of 80 to 99 wt% is obtained via adsorption on different types of activated carbon. No significant changes are observed when comparing mixtures without PS to those with 5 wt% PS. However, the strong effect of solvent choice is highlighted, where cyclohexene outperforms n-butyl acetate with differences in removal efficiency as high as 50 wt%. Furthermore, the use of computational modeling tools such as Gaussian16 and COSMO-RS is demonstrated to gain insight into the physicochemical properties of the FRs, which can optimize the purification system, including solvent choice. Finally, applying the proposed treatment process to real-world plastic WEEE samples further proves the effectiveness of the purification, marking a significant step forward in the dissolution recycling of plastics.

1. Introduction

Among the countless materials that have shaped our world, plastics stand unmatched. Their incredible versatility, durability, and affordability have transformed industries ranging from packaging and healthcare to construction and electronics [1,2]. Yet, this ubiquity comes at a price: a mounting environmental burden that demands urgent attention [3–10]. While the latter is currently widely recognized, leading to ambitious sustainability goals such as those outlined by the European Commission in the European Green Deal, this has not yet translated to an increase in plastic recycling rates proportionate to their production [11,12]. With global plastic production exceeding 400 Mt in 2022, less than 10% originates from recycled plastics. Looking at Europe, with a total plastic production of about 14% of the global share, approximately 13% is produced from recycled content. All other plastics end up in incineration, landfill, or the environment, thus not retaining their valuable carbon-based backbone in the lifecycle, which is essential to achieve true plastics circularity [13–15].

Of the 13% of European recycled plastic production in 2022, over 95% is derived from mechanical recycling [13]. The latter converts the plastic material into recyclate through mechanical force and heat, which includes sorting, shredding, washing, and extrusion, yet without (intentionally) changing the chemical structure and composition of the

* Corresponding author.
E-mail address: steven.demeester@ugent.be (S. De Meester).

https://doi.org/10.1016/j.cej.2025.164504
Received 14 February 2025; Received in revised form 1 June 2025; Accepted 3 June 2025
Available online 20 June 2025

plastic material. Therefore, additives and contaminants incorporated in the polymer matrix are not removed, indicating that the recyclate quality is highly dependent on the input quality of the plastic waste. Hence, mechanical recycling is often limited to plastic waste streams that can be adequately sorted and are free of contaminants, which are particularly scarce [16,17]. In fact, in order to qualify for high-quality mechanical recycling, plastic waste requires polymer purities above 90 to 95% [18]. The immiscibility of certain polymer types and the occurrence of thermal–mechanical degradation during processing further limits the applicability of mechanical recycling [17,19]. As a result, chemical recycling is often proposed to deal with heterogeneous and more complex plastic waste streams, such as multilayer materials. However, chemical recycling, involving either depolymerization (e.g., hydrolysis, glycolysis, and aminolysis) or thermal degradation (e.g., pyrolysis and gasification), results in lower yields with generally higher energy demands, while the presence of certain contaminants still proves to be problematic [17–25]. For instance, during thermal degradation, flame retardants (FRs) can act as precursors for the formation of hazardous compounds, among other things [26–30]. In catalytic pyrolysis, deactivation or blocking of the catalyst may also occur, together with corrosion and excessive coke formation [17,20,31,32].

Therefore, dissolution or solvent-based recycling offers an interesting alternative, where one uses the (selective) solubility of the polymers to free their matrix from contaminants and additives without breaking the carbon chains. In general, dissolution recycling – which in some cases can be considered a form of advanced mechanical or 'physical' recycling – can be performed via two different approaches. The first one is called dissolution-precipitation, where the plastic mixture is first dissolved and subsequently purified upon precipitation, which in turn can be done by cooling, evaporation, or adding an antisolvent. The second approach essentially entails a non-aqueous washing, where the plastic mixture is not dissolved but rather treated with a solvent to extract the undesired compounds [33–36]. However, it is particularly challenging to remove relatively large (undissolved) substances (e.g., inorganic additives) via such non-aqueous washing processes as their migration in the polymer matrix will remain fairly limited. Therefore, typical applications of this second approach are the removal of volatile organic compounds (VOCs) in deodorizing processes or targeting adhesives in delamination processes [21,37,38]. In dissolution-precipitation processes, all types of contaminants and additives can theoretically be removed from the mixture before precipitation of the polymer to avoid re-incorporating these undesired substances in the polymer matrix. Typically, filtration is applied to filter out these compounds, but this does not remove dissolved substances (e.g., non-polar organic additives), which include many plastic additives [39]. One example of additives that receive much attention towards removal is (brominated) flame retardants [33,40].

The persistence of these substances in recycled materials is deemed problematic due to the associated health risks, while they make up a substantial fraction of certain polymeric waste types [41,42]. It was shown that for Waste Electrical and Electronic Equipment (WEEE), for instance, approximately 16% of published concentrations exceeded the regulatory limit of 1000 mg kg^{-1} for brominated flame retardants (BFRs) [43]. Conventional mechanical recycling approaches are unable to remove these persistent organic pollutants (POPs) [17,26,44–46]. Indeed, BFRs and phosphorus flame retardants (PFRs) have been reported in children's toys, among others, while their (neuro)toxic properties have been described in the literature [47–54]. In light of these concerns, it becomes imperative to address the removal of FRs during recycling processes.

This work focuses on five different flame retardants, including BFRs and PFRs, while covering both restricted and alternative compounds. Hexabromocyclododecane (HBCD) and tetrabromobisphenol A (TBBPA) are selected as BFRs, triphenyl phosphate (TPHP) as PFR, and decabromodiphenyl ethane (DBDPE) and PolyFR as alternative FRs. The latter compound consists of a brominated butadiene/styrene block copolymer, developed as an alternative for HBCD with a better proclaimed environmental and health profile, while DBDPE is currently one of the most commonly used novel BFRs (NBFRs) [41,55]. All of the aforementioned concerning (i.e., TBBPA and TPHP) and restricted (i.e., HBCD with a low POPs content level (LPCL) of 0.1 wt% in waste streams and an unintentional trace contaminant (UTC) limit of 0.01 wt% in recyclates (Regulation (EU) 2019/1021 Annex I)) flame retardants are commonly found in WEEE [56]. Moreover, concerns about the toxicity of NBFRs such as DBDPE are growing substantially [57,58]. Furthermore, insights from industry consultation indicate that all five flame retardants have been prevalent in PS applications with HBCD being historically present.

As mentioned, typical dissolution recycling processes involve filtration to remove undissolved additives. However, a crucial question arises: which additives are actually dissolved and which remain undissolved? This study observes that some FRs are indeed undissolved, whereas others can be dissolved, which implies that removal of (brominated) flame retardants might at least need two cleaning techniques. For this reason, we propose a combination of filtration and adsorption for the removal of both undissolved and dissolved FRs during the dissolution recycling of plastic. Adsorption is a widely adopted separation technique for the treatment of wastewater. However, its adoption in non-aqueous systems, particularly in a solvent-based recycling context, remains largely unexplored. A first exploration was made in earlier work, where the adsorption behavior of a red dye in different polystyrene solutions was investigated, demonstrating the potential of adsorption as an effective dissolution recycling technique for the removal of plastic additives [59]. In this context, this study is the first to systematically investigate the solubility of various types of flame retardants using both experimental methods and molecular modeling. Furthermore, building on these insights, a combined purification method is proposed. This method, which includes a comparative evaluation of the effectiveness of different adsorbents, demonstrates highly efficient removal of different types of flame retardants, even from real waste samples.

Summarizing, the present work investigates the removal of FRs by dissolution recycling, proposing a combination of filtration and adsorption. In this context, we focus on polystyrene (PS), a prominent polymer type comprising 5 to 6% of the global plastic production and an important polymer in WEEE streams, often containing FRs [13]. For the dissolution of PS, this study compares n-butyl acetate, which we used in a previous study, with cyclohexene, which in turn was found to dissolve the highest amount of PS in a fixed time interval among more than 30 different solvents [59,60]. Cyclohexene is an aliphatic cycloalkene, while butyl acetate is a type of ester with a significantly higher polarity. To characterize the FRs and simulate their solubility in the selected solvents, the conductor like screening model for real solvents (COSMO-RS) combined with the computational chemistry software packages Gaussian16 and RDKit was applied. Based on the solubility results, the FRs were removed either by filtration or adsorption. In addition, this study includes a case study on actual WEEE samples to demonstrate the applicability of the proposed cleaning methods.

2. Materials and methods

2.1. Materials

The flame retardants HBCD and PolyFR were kindly provided by Neue Materialien Bayreuth GmbH. The latter is also known under the trade name FR-122P. Centexbel supplied DBDPE, whereas the other FRs, namely TBBPA and TPHP, were purchased from Merck KGaA. All FRs came in solid form. The first type of activated carbon (i.e., AC-01) was also purchased from Merck KGaA, while the other two types (i.e., AC-84 and AC-87) were provided by DESOTEC. The solvents n-butyl acetate and cyclohexene, both with a purity of 99%, were procured from Thermo Fisher Scientific Inc. Lastly, the polymer was kindly provided by INEOS Styrolution in the form of general purpose polystyrene (GPPS) pellets, GPPS 168N.

2.2. Preparation of adsorbents

The activated carbon materials were individually crushed in an Anton Paar BM500 ball mill for 1.5 minutes at 7.00 Hz to obtain fine powders. The powders were subsequently sieved for the fraction between 32 and 45 μm particle size. Before the experiments, the powders were dried in an oven at 368 K for 12 h and cooled down to room temperature in a desiccator. The latter to prevent airborne contaminations, for example by water vapor.

2.3. Characterization of adsorbents

Nitrogen adsorption–desorption isotherms were constructed for the adsorbent materials by using a Micromeritics Tristar II 3020 Analyzer operated at 77 K. The specific surface area (S_{BET}) was calculated via a Brunauer–Emmett–Teller (BET) analysis. At the same time, the t-plot method was used to determine the external surface area (S_{ext}), the micropore area (S_{micro}), the total pore volume (V_{tot}), and the micropore volume (V_{micro}) [61,62]. The average pore width was estimated via the Barrett–Joyner–Halenda method (W_{avg}) [63]. A scanning electron microscopy (SEM) analysis was performed with a JEOL JSM-7600F to investigate the surface morphology of the adsorbent materials. Furthermore, Fourier transformed infrared spectroscopy (FTIR) was used to identify changes in surface chemistry before and after adsorption, using a Nicolet iS20 FTIR Spectrometer. Lastly, pH measurements were taken from aqueous mixtures containing 20 mL of distilled water and 2 g of adsorbent material. Additionally, a Boehm titration was performed to determine the amount of acidic and basic groups on the surface of the adsorbents.

2.4. Characterization of flame retardants

For convenience, the chemical structures of the flame retardants are shown again in Fig. 1. Physicochemical properties of these compounds were estimated using the computational chemistry software packages of Gaussian16 and RDKit, in combination with COSMO-RS [64–66]. For each flame retardant, Gaussian16 was used to optimize the geometry of the corresponding molecular structure by utilizing a set of finite wavefunctions to describe the electronic state of the molecule. To that end, 1000 conformers were initially generated via the RDKit package within the Jupyter Notebook environment. Conformers are different spatial arrangements of distinct groups of atoms of a particular molecule created by allowing rotation around certain bonds. The conformers were subsequently pruned based on their level of similarity. For each of the remaining conformers, the universal force field (UFF) method was utilized for geometry optimization and, subsequently, to calculate the total energy to identify the conformer with the lowest energy (i.e., the most stable arrangement of atoms for the molecule). Ultimately, this conformer defined the starting point of the geometry optimization performed in Gaussian16. Next, the common method/basis set of B3LYP/6-311++G(d,p) combined with Grimme's D3 dispersion correction (i.e., DFT-D3) was used to optimize the initial geometry and to subsequently perform a frequency calculation to check for imaginary frequencies [67–69]. Afterward, a Self-Consistent Reaction Field (SCRF) single-point energy calculation was performed to account for the solvation effect, which generated the input file for the COSMO-ThermX software [70]. This file included the charge distribution of the optimized geometry, which was then converted into its sigma profile. The sigma profile constitutes the main input for the thermodynamic model COSMO-RS. It describes the interactions between the FRs and the selected solvents, eliminating the need for experimental data to regress binary interaction parameters and estimate activity coefficients in multi-component systems. All described calculations were performed via high-performance computing (HPC) on a 2x 48-core AMD EPYC 7552 processor supercomputer with a total of 128 worker nodes.

Table 1
Overview of the most important input data for COSMO-RS, experimentally obtained via DSC analysis.

Compound	T_m (°C)	ΔH_{fusion} (kJ mol^{-1})
HBCD	179	29
TBBPA	182	34
DBDPE	349	66
TPHP	52	30
PolyFR	244	32 479

The first property of interest is about the dimensions of the molecular structure. It comprises two metrics: the smallest (d_{min}) and the largest diameter (d_{max}) of a circle that can encompass the molecule, given that this diameter must not exceed the maximum distance between two atoms of the molecule. Essentially, d_{min} (i.e., lower size limit) represents the smallest diameter of a cylinder, indicative of an adsorbent pore, through which the molecule can physically diffuse given a precise orientation. In contrast, d_{max} (i.e., upper size limit) dictates the smallest diameter of a cylinder that can accommodate the diffusion of the molecule irrespective of its momentary orientation. To calculate these metrics, a three-dimensional (3D) shape is fitted around the optimized molecular structure (i.e., its convex hull), established earlier via Gaussian16. Next, a series of 10,000 distinct points of view (POVs) is defined via a helix trajectory that rotates 300 times around the 3D structure, covering the entire molecule with its center coinciding with the origin point of the cartesian coordinate (Fig. 2). Each POV forms a particular axis with this origin point. Subsequently, a two-dimensional (2D) projection of the molecular structure on a plane perpendicular to this axis is established, after which the widest distance of the molecule (d_i) is determined by iterating through the distances between the projected points. This process is repeated for each POV or – in other words – for each potential molecule orientation. Ultimately, d_{min} is defined by the minimum value of di across all POVs, whereas d_{max} is determined by the corresponding maximum value. These calculations were performed in Python within the Jupyter Notebook environment.

The second property is the dipole moment (μ), which provides a quantitative measure of polarity, given that it represents the vectorized result of charge, either negative or positive, stemming from potential differences in electronegativity within the molecule. The dipole moment is a direct result of the COSMO-RS analysis elaborated earlier. The third and final property of interest is the absolute solubility (S) of the FRs in both n-butyl acetate and cyclohexene at a temperature of 293 K, calculated via COSMO-RS. However, the latter requires additional input data, among which the melting point (T_m) and the heat of fusion (ΔH_{fusion}) are the most essential. Therefore, a differential scanning calorimetry (DSC) analysis was performed from 0 to 550 ° C at 10 ° C min^{-1} on all the FRs. A summary of the input data for COSMO-RS is provided in Table 1. In addition, for PolyFR, which is the most complex structure to model due to its polymeric nature, a gel permeation chromatography (GPC) analysis was performed to determine its average molecular mass, resulting in 163 627 g mol^{-1}. The Supplementary Information (Figure S1) provides a visual representation of those results.

The solubility in n-butyl acetate and cyclohexene was also validated experimentally by gradually increasing the FR concentration at 293 K to the point where solid (precipitated) particles remained visually undissolved for at least 24 h (i.e., the solution turned cloudy). During dissolution, the mixtures were continuously stirred at 300 rpm. Afterward, the mixtures were filtered and centrifuged at 4500 rpm for 20 min. The supernatant was subsequently analyzed via thermogravimetric analysis (TGA) to determine the solubility using the Netzsch TG 209 F3 Tarsus. Moreover, TGA was also performed on all FRs individually. All experiments were performed in duplicate.

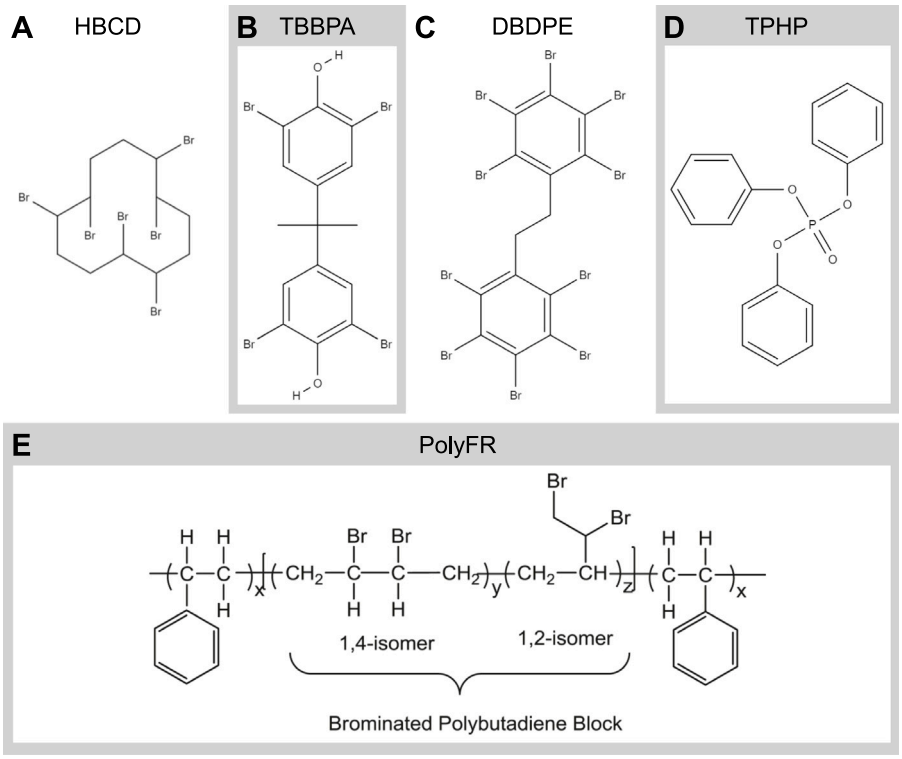

Fig. 1. Chemical structure of (A) hexabromocyclododecane, (B) tetrabromobisphenol A, (C) decabromodiphenyl ethane, (D) triphenyl phosphate, and (E) the brominated polymeric flame retardant PolyFR.

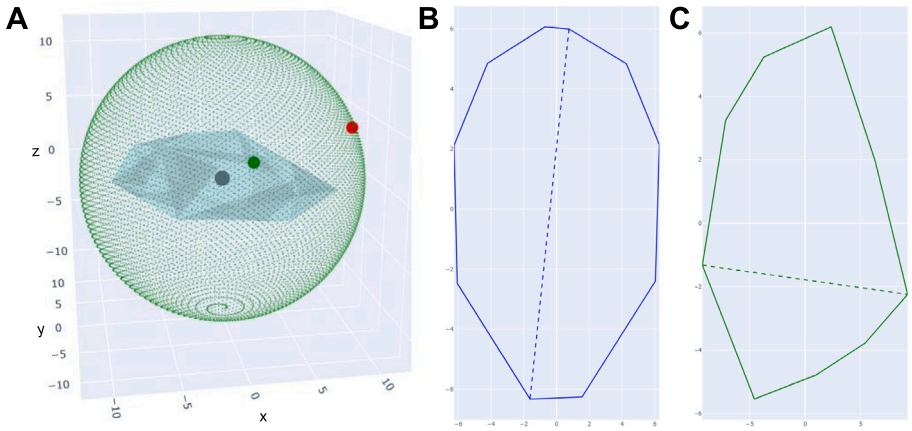

Fig. 2. Representation of (A) the 3D convex hull fitted around the optimized molecular structure with the surrounding small green dots defining the simulated POVs, where the big black dot identifies the center point (0,0,0), the big red dot the POV that corresponds with the lower size limit d_{min}, and the big green dot the POV that corresponds with the upper size limit d_{max}, (B) the 2D projection of the molecular structure on a plane perpendicular to the axis formed by the center point and the POV that corresponds to the big red dot in (A) with the blue dashed line representing d_{min}, and (C) the 2D projection of the molecular structure on a plane perpendicular to the axis formed by the center point and the POV that corresponds to the big green dot in (A) with the green dashed line representing d_{max}. This for the case of HBCD as an example.

2.5. Filtration experiments

Before the filtration experiments, a particle size distribution (PSD) analysis was performed to identify the optimal pore size for the membrane. This was done for the FRs with poor solubility in n-butyl acetate and/or cyclohexene (i.e., S < 0.01 wt%). Suspensions with a FR concentration of 0.25 wt% were selected, considering that these compounds are typically added to PS applications in a range of 1 to 15 wt%, where the recommended polymer concentration for dissolution-based recycling typically lies around 5 to 10 wt% [42]. The PSD was measured using a Malvern Mastersizer S, a static laser diffraction analyzer.

Afterward, membrane filtrations were performed on similar suspensions of 50 mL with a FR concentration of 0.25 wt%, without and with addition of 5.0 wt% PS. The filtrations were carried out in a Sterlitech HP4750X cell, which was magnetically stirred at 500 rpm and connected to a compressed nitrogen tank. This dead-end filtration setup was operated at 293 ± 1 K with a constant pressure of 1.0 ± 0.1 bar. The volumetric flux was measured, and the feed and the filtrate were analyzed via TGA to determine the removal efficiency. If the thermal degradation of one of the FRs occurred over the same temperature interval as that of PS, rendering quantification via TGA challenging, turbidity measurements were used as an alternative. For a detailed description of this methodology, the reader is referred to Kol et al. (2023) [71]. Upon termination of the filtration, the membrane was removed from the cell for further analysis. A schematic overview of

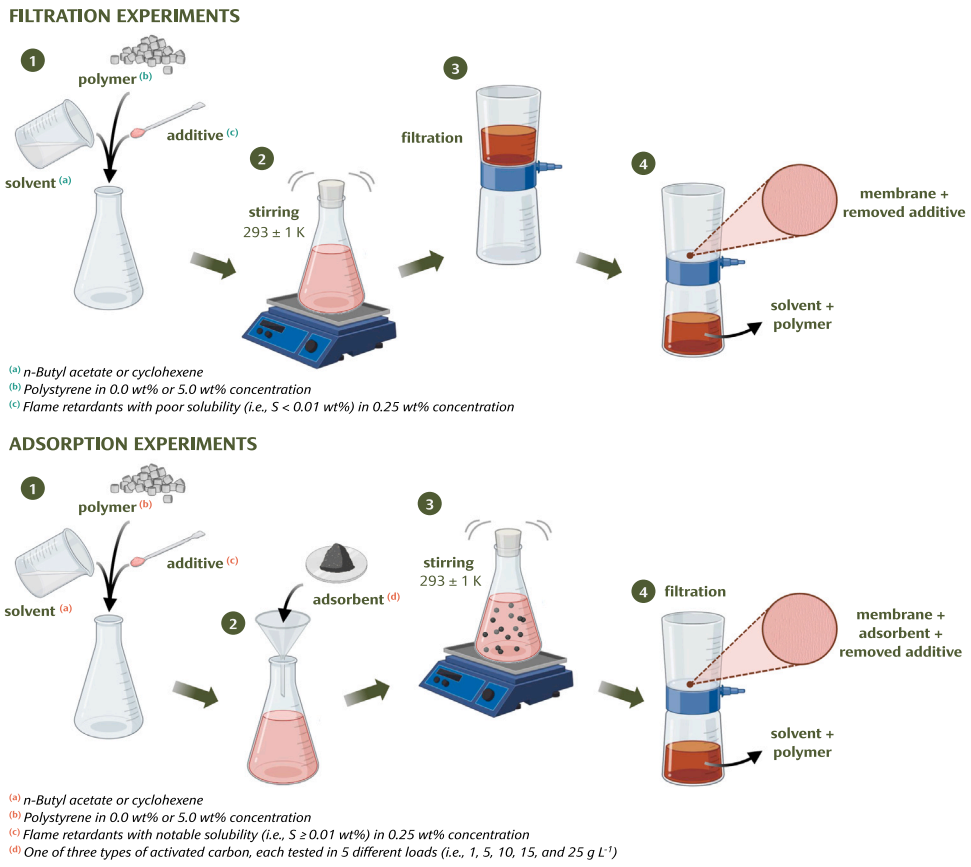

Fig. 3. Schematic overview of the conducted experiments.

the experimental flow is provided in Fig. 3. Again, all experiments were performed in duplicate to ensure reproducibility of the results.

Although not the focus of this work, membrane fouling was also investigated as it is a crucial issue in the industrial application of membrane technology. The latter is primarily due to the associated decline in overall flux, the reduced membrane service life, and increased operational costs [72]. Several models have been proposed in the literature to describe the membrane fouling behavior by predicting the variations in flux. In general, four basic mechanisms can be distinguished [73]. The first one is complete blocking, where each membrane pore is completely closed by an individual deposited particle, while particles never settle on top of each other (i.e., no cake formation). The second one is intermediate blocking, which is less restrictive than the former. It states that particles may settle on previously deposited particles and, therefore, not always cause blocking of a membrane pore upon arriving at the membrane surface. The third one is standard blocking, where the particles are deposited inside the membrane on the pore walls, causing narrowing of the pores over time. The fourth and final one is called cake filtration, in which case the particles accumulate on the surface of the membrane and form a cake layer [74]. A summary of these four basic models is given in Table 2. More complex models exist that account for the simultaneous occurrence of different fouling mechanisms or their variation over time, yet these lie beyond the scope of this work [72]. All model parameters were calculated in R with the Flexible Modelling Environment (FME) package by means of a nonlinear regression with the Levenberg–Marquardt and pseudorandom-search algorithms, minimizing the sum of squares error (SSE) (Eq. (1)) [75]. Furthermore, a combination of two different statistical measures was used to evaluate the model performance, the universal coefficient of determination (R^2) and the Akaike's information criterion (AIC), given by Eq. (2) and (3), respectively.

$$SSE = \sum_{i=1}^{N} \left(y_{i,cal} - y_{i,exp}\right)^2 \tag{1}$$

$$R^2 = 1 - \frac{\sum_{i=1}^{n} \left(y_{i,exp} - y_{i,cal}\right)^2}{\sum_{i=1}^{n} \left(y_{i,exp} - \overline{y_{i,exp}}\right)^2} \tag{2}$$

$$AIC = N\ ln\left(\frac{SSE}{N}\right) + 2N_p + \frac{2N_p\left(N_p+1\right)}{N-\left(N_p+1\right)} \tag{3}$$

where $y_{i,cal}$ is the calculated value of the dependent variable, $y_{i,exp}$ is the experimental value of the dependent variable, $\overline{y_{i,exp}}$ is the average of the experimental values of the independent variable, N is the number of data points, and N_p is the number of parameters of the model.

2.6. Adsorption experiments

Adsorption experiments were performed on the FRs demonstrating notable solubility in n-butyl acetate and/or cyclohexene (i.e., S ≥ 0.01 wt%). Analogous to the filtration experiments, the initial FR concentration was 0.25 wt%. In the first iteration, no PS was added to the mixture, whereas in the second iteration, 5.0 wt% PS was included for the most promising solvent/adsorbent combination. For both iterations, solutions of 20 mL were prepared in glass vials with increasing adsorbent dose, specifying five different adsorbent concentrations of 1, 5, 10, 15, and 25 g L^{-1}. To that end, three adsorbent materials (i.e., AC-01, AC-84 and AC-87) were considered. Prepared solutions were carefully sealed and shaken at 120 rpm at a temperature of 293 ± 1 K, for at least 24 h to ensure the equilibrium state was reached (i.e., FR concentration remained constant for three consecutive measurements). Afterward, the samples were filtered through a 0.45 μm PTFE membrane to separate the solid from the liquid phase.

The filtrate was analyzed by a Shimadzu GCMS-QP2020 NX gas chromatography-mass spectrometer (GC–MS) equipped with an Agilent HP-5 ms capillary column (30 m × 0.25 mm ID, 0.25 μm thickness, with a temperature limit of −60 °C to 325 °C) and coupled to an

Table 2
Overview of the four basic fouling models considered for the filtration part of this work.

Name	Equation	Fitted parameter	Reference
Complete blocking	$V = \frac{J_0}{K_b}\left(1 - exp\left(-K_b t\right)\right)$	K_b	[76]
Intermediate blocking	$V = \frac{1}{K_i} ln\left(1 + K_i J_0 t\right)$	K_i	[76]
Standard blocking	$V = \left(\frac{1}{J_0 t} + \frac{K_s}{2}\right)^{-1}$	K_s	[76]
Cake filtration	$V = \frac{1}{K_c J_0}\left(\left(1 + 2K_c J_0^2 t\right)^{0.5} - 1\right)$	K_c	[76]

where V is the accumulated permeate volume ($m^3\ m^{-2}$), J_0 the initial flux ($m^3\ m^{-2}\ h^{-1}$), K_b the complete blocking constant (s^{-1}), K_i the intermediate blocking constant (m^{-1}), K_s the standard blocking constant (m^{-1}), and K_c the cake filtration constant ($s\ m^{-2}$).

OPTIC-4 pyrolysis unit. An AOC-6000 Plus autosampler was used in combination with this pyrolysis-GC-MS configuration. For each FR, the GC–MS method and the pyrolysis program were first optimized, after which the corresponding calibration curves were established. A detailed overview of this, including the applied temperature profiles, can be consulted in the Supplementary Information (Table S1–S2 and Figure S2–S4). Samples of 10 μL were carefully weighed, placed into a microvial, and subsequently loaded onto the pyrolysis-GC-MS. With respect to the treated samples that contained PS, an additional TGA was performed to investigate the adsorption behavior of the polymer itself, using the Netzsch TG 209 F3 Tarsus. A schematic overview of the experimental flow is provided in Fig. 3. All experiments were duplicated for reproducibility purposes, and the pyrolysis-GC-MS measurements were performed in triplicate.

A semi-quantitative methodology was applied to evaluate the purification potential of the adsorption process. The removal efficiency (RE) was calculated as follows:

$$RE = \frac{\frac{A_{in,FR}}{m_{in,FR}} - \frac{A_{out,FR}}{m_{out,FR}}}{\frac{A_{in,FR}}{m_{in,FR}}} \times 100 \quad (4)$$

where $A_{in,FR}$ represents the area of the characteristic peak(s) of the corresponding chromatogram of the initial concentration of the FR component, $A_{out,FR}$ represents the area of the characteristic peak(s) of the corresponding chromatogram of the FR component after the adsorption treatment, $m_{in,FR}$ is the sample mass of the initial concentration of the FR component, and $m_{out,FR}$ is the sample mass of the FR component after adsorption treatment. This semi-quantitative approach was selected since absolute quantification requires accurate calibration with pure standards, which can be fairly challenging for pyrolysis-GC-MS. However, verifying that the measurements lie within a linear region of the corresponding calibration curve remains important to avoid over- or underestimation. Therefore, as mentioned earlier, calibration curves were constructed before the start of the experiments.

2.7. Case study: WEEE samples

A large-scale sorting and recycling company located in Belgium, with a total plastic recycling capacity of 90,000 tons per year, provided two types of sorted WEEE samples. The first sample originated primarily from discarded refrigerators (i.e., WEEE Type 1), while the second sample was a mix of smaller electronic devices and household appliances (i.e., WEEE Type 2). Both samples were subjected to several processing steps onsite, primarily to fragment the material and remove ferrous and non-ferrous metals. These steps included separation techniques such as magnetic separation, eddy current separation, and density separation through sink/float operations. After a series of these density separations, samples were gathered from the respective plastic streams expected to contain primarily halogenated PS fractions.

To further reduce the sample mass, the coning and quartering methodology was applied for both samples types. To that end, the material was first dried, mixed, compacted into a cone, and subsequently flattened on a clean surface. Next, the material was divided into four equal sections (i.e., quadrants). Two opposing quadrants were randomly selected and combined, after which the process was repeated until the desired sample mass was obtained [77]. Here, a total mass of 250 g was selected for each sample type, which was then shredded into a powder using a Shini SG-1635 low-speed granulator in combination with an Anton Paar BM500 ball mill, aided by the addition of liquid nitrogen.

The prepared waste samples were first analyzed for FRs (i.e., the ones included in this work). This was done via pyrolysis-GC-MS, as elaborated earlier. Afterward, the waste samples were dissolved in the most optimal solvent, as revealed by the preceding investigation, meaning either in n-butyl acetate or cyclohexene. Similar to the filtration and adsorption experiments, a concentration of 5 wt% was selected with a total solution volume of 20 mL. After removing the undissolved substances via filtration (0.1 μm pore size PTFE membrane), a sample was taken from the filtrate to have an accurate baseline for the potential starting concentration of the (dissolved) FRs. The most optimal adsorbent type based on the results with the pure compounds was then added in a concentration of 25 g L^{-1} (i.e., either AC-01, AC-84 or AC-87). Prepared solutions were sealed and shaken at 120 rpm at a temperature of 293 ± 1 K for at least 24 h. Afterward, the samples were again filtered through a 0.45 μm pore size PTFE membrane to remove the adsorbent material. The filtrate samples were analogously analyzed via pyrolysis-GC-MS. To assess the performance of the proposed purification process on actual waste samples, the removal efficiency was ultimately determined via Eq. (4). Similarly, all experiments were performed in duplicate, and the measurements were triplicated.

3. Results and discussion

3.1. Characterization of flame retardants

A summary of the properties calculated using Gaussian16 and COSMO-RS is provided in Table 3. For the physical dimensions of the molecules, d_{min} fluctuates around 13 Å, while d_{max} is situated around 20 Å, except for the polymeric flame retardant PolyFR where no meaningful data could be generated in terms of molecular size. Indeed, due to the complexity of modeling organic polymers, especially triblock copolymers such as PolyFR, an oligomer of PolyFR was constructed consisting of three repeating monomers for each of the three monomer types, while minimizing steric hindrance. The latter is a common approach for modeling the behavior of polymer solutions using COSMO-RS [78]. Despite being unable to calculate size based on the oligomeric model, the corresponding polymers are expected to have an average size of 200 to 300 Å [79]. Regarding the polarity of the molecules, TBBPA and TPHP are found to be polar (i.e., μ > 1.0 D), while the structures of HBCD and DBDPE appear to have a negligible net dipole moment. Indeed, despite having relatively strong electronegative atoms (i.e., bromine), the 3D symmetry of these latter molecules cancels out the individual bond dipole moments within the respective structures. This can be visually derived by plotting the sigma profiles on top of the chemical structures of the FRs, which is illustrated in Fig. 4.

The sigma profiles generated via COSMO were further analyzed and are available in the Supplementary Information (Figure S5). These profiles represent the distribution of surface charge densities (σ) and

Table 3
Summary of the flame retardant (FR) properties[a] estimated by means of Gaussian16 and COSMO-RS.

FR	d_{min} (Å)	d_{max} (Å)	μ (D)	S_{mod} (wt%)		S_{exp} (wt%)	
				n-butyl acetate	cyclohexene	n-butyl acetate	cyclohexene
HBCD	12.99	18.54	0.00	34.16	0.74	7.92 ± 0.42	1.10 ± 0.10
TBBPA	13.22	20.08	3.52	9.70	1.76	41.98 ± 2.26	2.98 ± 0.55
DBDPE	12.81	19.73	0.01	0.00	0.00	0.00 ± 0.00	0.00 ± 0.00
TPHP	15.34	23.79	1.28	58.14	46.48	51.36 ± 3.17	33.97 ± 2.97
PolyFR	NA	NA	NA	NA	NA	40.50 ± 0.71[b]	0.00 ± 0.00

[a] d_{min}: lower pore size limit, d_{max}: upper pore size limit, μ: net dipole moment, S_{mod}: absolute solubility estimated using COSMO-RS at a temperature of 293 ± 1 K, S_{exp}: absolute solubility experimentally derived at a temperature of 293 ± 1 K.

[b] Gel formation was observed

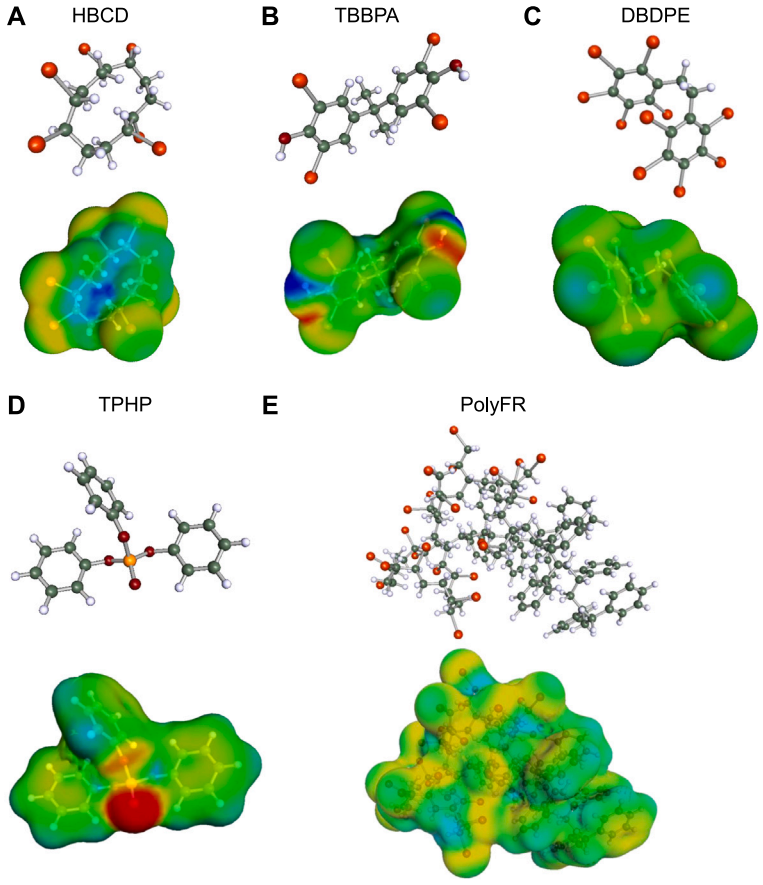

Fig. 4. Visualization of the 3D chemical structure and the corresponding surface-charge density via the sigma profile of (A) HBCD, (B) TBBPA, (C) DBDPE, (D) TPHP, and (E) PolyFR, generated via COSMO-RS.

serve as a valuable tool for predicting the solubility behavior and molecular polarity. Different regions of the sigma profile correspond to distinct polar characteristics, where the polar regions are associated with hydrogen-bond donor capacities (i.e., σ typically lower than -0.0082 e Å^{-2}) or hydrogen-bond acceptor capacities (i.e., σ typically greater than 0.0082 e Å^{-2}) [80]. A pronounced hydrogen-bond acceptor peak was observed in n-butyl acetate, TBBPA, and TPHP. For cyclohexene, this feature is comparatively less intense, and completely absent for HBCD, DBDPE, and PolyFR. Conversely, a clear hydrogen-bond donor region was present across all components (i.e., all flame retardants and solvents), with HBCD and TBBPA showing a broader donor range. The good solubility observed for some flame retardants might thus be attributed to favorable intermolecular hydrogen bonding, arising from (i) a match between the donor-rich regions of the flame retardant and the acceptor-rich profile of the solvent (e.g., HBCD, TBBPA, and TPHP in n-butyl acetate), or (ii) a match between the acceptor-rich regions of the flame retardant and the donor-rich profile of the solvent (e.g., TPHP in cyclohexene). This demonstrates how sigma profiles not only indicate overall polarity, but also reveal the specific types of molecular interactions, such as hydrogen bonding, that govern solubility and compatibility in solvent selection. Overall, it may be concluded that solvents with pronounced hydrogen-bond acceptor capacities, such as n-butyl acetate, exhibit strong molecular affinity towards the BFRs, thereby impeding their effective removal from the dissolution system. In contrast, solvents with weaker hydrogen-bond acceptor capacities, such as cyclohexene, exhibit less pronounced interactions with the BFRs, which benefits their removal.

The experimental results of the solubility tests are also given in Table 3. In general, it can be seen that the solubility of the FRs in cyclohexene is lower compared to n-butyl acetate. Moreover, DBDPE and PolyFR are practically insoluble in cyclohexene at the selected conditions. Both findings are consistent with the predictions generated via COSMO-RS. Despite being unable to calculate absolute solubility data for PolyFR, relative solubility data shows a much lower affinity of PolyFR for cyclohexene compared to n-butyl acetate (Table S3), suggesting that PolyFR is practically insoluble in the former. In other

words, the model successfully identified the FRs that are undissolved (i.e., S < 0.01 wt%) versus those that are dissolved. However, it can be observed that the predictions by COSMO-RS deviate from the experimental solubility of the FRs. In particular, the discrepancies for HBCD and TBBPA are high. This can be explained by the limitations of the B3LYP/6-311++G(d,p) model used by Gaussian16 to minimize the total energy of the molecular structures. Alternatively, the FRs might have multiple stable conformers that coexist, where COSMO-RS would be unable to capture the variations in their respective properties. To improve the predictions, the model was extended for the case of HBCD by using higher-order polarization functions, resulting in B3LYP/6-311++G(3pd,3df). Actually including multiple conformers would require an extensive amount of additional computation power and therefore lies outside the scope of this work.

The prediction results for HBCD of the extended model indicate an absolute solubility of 31.96 wt% in n-butyl acetate and 1.07 wt% in cyclohexene. For cyclohexene, this is in line with the experimental results. For n-butyl acetate, however, this represents only a slight improvement and remains inaccurate, as there is still a relative difference of 75 % compared to the experimental data. The latter might suggest that the commonly used B3LYP/6-311++G(d,p) model is not well suited to quantify absolute solubilities of some FRs, i.e., organic molecules with a considerable amount of heavy (halogen) elements such as bromine. A concurrent possibility is that some of the molecules do demand the inclusion of multiple low-energy conformers to adequately determine their absolute solubility. The latter would require an additional clustering step after the conformational search to identify representative structures, each of which would then undergo geometry optimization. This process significantly increases computational demand and was therefore considered beyond the scope of the present study. However, aside from predicting the absolute solubility, referring to the maximum amount of solute that can dissolve in a solvent under specific temperature and pressure conditions (expressed in wt%), COSMO-RS can also generate relative solubilities. In that case, the model predicts the solubility of a solute in different solvents relative to each other rather than providing an exact numerical value for the solubility in a specific solvent. This is particularly useful when the aim is to identify the most optimal solvent during a screening process, such as in the optimization of the proposed treatment process in this work. The relative solubilities of the FRs for n-butyl acetate and cyclohexene calculated via COSMO-RS (Table S3) are consistent with the experimental data, demonstrating its practical value.

3.2. Removal of undissolved flame retardants

Considering the solubility results of the FRs, filtration experiments were performed on separate suspensions of DBDPE and PolyFR in a concentration of 0.25 wt% with cyclohexene as solvent. PS was not added in the first stage, whereas in the second stage, 5.0 wt% PS was dissolved in the mixtures. To that end, the PSD of these suspensions was determined, as depicted in the Supplementary Information Figure S6. This shows that the DBDPE particles follow a bimodal distribution, possibly due to aggregation or coalescence, while the PolyFR particles present an unimodal distribution. In both cases, the smallest particles were detected around 0.2 μm. This information is used to identify the most optimal membrane for the subsequent filtration experiments and – by extension – for optimizing centrifugation processes as an alternative separation technique for such solid/liquid systems.

Based on the PSD, a solvent-resistant PTFE membrane with a pore size of 0.1 μm and a thickness of 30 μm (Omnipore JVWP09025) was selected for the filtration experiments. Initially, no PS was added to the suspensions, and the TGA results indicate near complete removal of both FRs (i.e., RE > 99.5 wt%) (Table 4). This is in line with expectations, as these predominantly undissolved substances with a particle size larger than 0.2 μm should indeed be retained by a membrane with a pore size of 0.1 μm. Similar results were obtained for the mixtures containing 5.0 wt% PS. However, due to the overlap in the TGA degradation peaks of DBDPE and PolyFR with PS, the removal efficiencies in this case were determined via turbidity measurements. The corresponding calibration curves can be consulted in the Supplementary Information (Figure S7). Again, a removal efficiency higher than 99.5 wt% was achieved for both DBDPE and PolyFR mixtures, with a respective standard deviation of 0.1 and 0.2 wt%.

Table 4
Summary of the experimental results for the removal efficiency (RE) of DBDPE and PolyFR from cyclohexene mixtures in a concentration of 0.25 wt% without or with addition of 5.0 wt% PS, using a dead-end filtration operated at 1.0 ± 0.1 bar and 293 ± 1 K with a 0.1 μm pore size PTFE membrane.

Mixture	RE (wt%)
DBDPE	99.6 ± 0.4
DBDPE + PS	99.8 ±0.1
PolyFR	99.5 ± 0.4
PolyFR + PS	99.6 ± 0.2

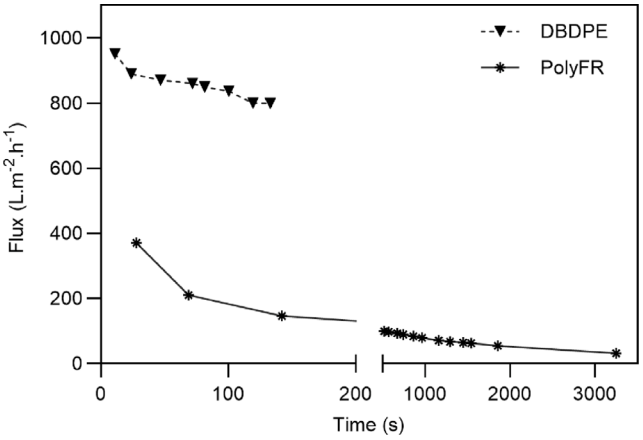

Fig. 5. Filtration flux of cyclohexene mixtures of DBDPE (*dashed line with reversed triangles*) and PolyFR (*solid line with asterisks*) in a concentration of 0.25 wt%.

Furthermore, the changes in flux through the membrane were investigated as a function of time (Fig. 5). The flux for the DBDPE mixtures was significantly higher than for the PolyFR mixtures, meaning that the filtration of the PolyFR particles was more hindered than the DBDPE particles. To better understand the fouling mechanism responsible for this behavior, the experimental data was fitted by means of the four basic membrane fouling models (Table 2). A summary of the modeling results is given in Table 5. For the DBDPE and PolyFR mixtures, the complete fouling model describes the system's behavior best, with an R^2 of 0.99 and 0.89, respectively. Indeed, the particle size of the FRs is significantly larger than the membrane's pore size. At the same time, the formation of a cake layer is largely avoided by the continuous stirring and the relatively low mass fraction of solids in the feed. However, it must be noted that for the DBDPE mixtures, the description by all the analyzed fouling models is good (i.e., $R^2 > 0.99$). This can be due to two main reasons: (1) the actual fouling mechanism involves a combination of the phenomena described by the different models, which are not mutually exclusive, or – more likely – (2) the experimental data is not sufficiently discriminating to differentiate between the models, which is supported by the fact that in general little fouling is observed for the DBDPE mixtures. The latter is associated with the relatively high accumulation rate of permeate volume, making it particularly challenging to capture the onset of the actual fouling behavior given the limited suspension volume. Therefore, future research should include a more detailed analysis of the fouling behavior to facilitate large-scale implementation.

Ultimately, successful removal of the undissolved FRs by means of filtration is achieved. Next to filtration, however, centrifugation

Table 5
Modeling results of the four basic fouling models for the filtration of cyclohexene mixtures of DBDPE and PolyFR in a concentration of 0.25 wt%.

Model	Parameter	DBDPE	PolyFR
Complete blocking	K_b (s^{-1})	3.2×10^{-3}	7.2×10^{-3}
	R^2	0.999	0.891
	AIC	−202.94	−225.56
Intermediate blocking	K_i (m^{-1})	1.3×10^{1}	2.1×10^{2}
	R^2	0.998	0.871
	AIC	−201.24	−222.53
Standard blocking	K_s (m^{-1})	1.3×10^{1}	1.1×10^{2}
	R^2	0.998	0.834
	AIC	−201.16	−217.93
Cake filtration	K_c (s m^{-2})	5.7×10^{4}	1.0×10^{7}
	R^2	0.998	0.500
	AIC	−199.16	−198.08

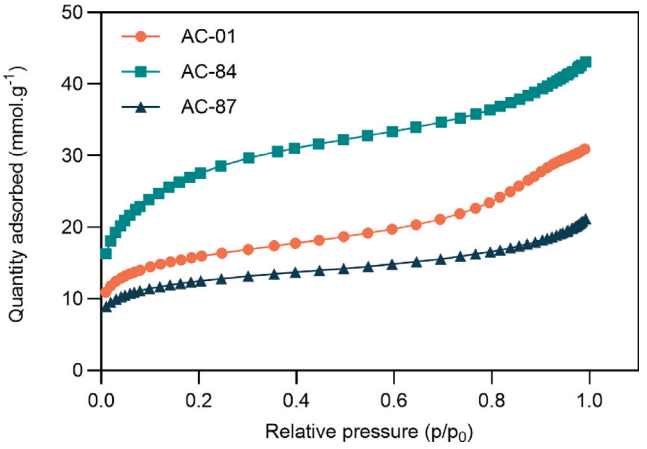

Fig. 6. Nitrogen adsorption isotherms of the activated carbons AC-01 (*orange circles*), AC-84 (*green squares*), and AC-87 (*dark blue triangles*) performed at a temperature of 77 K.

is also a viable option for the removal of undissolved substances in dissolution recycling of PS, as investigated by Kol et al. (2023) [71]. Therefore, in this study, it was additionally demonstrated that a near complete removal (i.e., RE > 99.5 wt%) of both DBDPE and PolyFR can be attained by centrifugation at 4500 rpm for 1 min, despite the significant increase in viscosity due to the dissolution of PS. A more detailed description of the centrifugation experiments and their results is provided in the Supplementary Information (Table S4–S6).

3.3. Removal of dissolved flame retardants

3.3.1. Characterization of adsorbents

The nitrogen adsorption isotherms are depicted in Fig. 6, with a summary of the different characteristics of the adsorbent materials in Table 6. From this, it is evident that AC-84 has the highest specific surface area S_{BET} with 2164 m^2 g^{-1} compared to 1214 and 947 m^2 g^{-1} for AC-01 and AC-87, respectively. Furthermore, AC-84 has the highest total pore volume V_{tot}, yet the lowest micropore volume V_{micro}, where only about 14% of its total pore volume is occupied by micropores compared to 24 and 31% for AC-01 and AC-87, respectively. Similarly, the micropore surface area S_{micro} is the lowest for AC-84 among the three activated carbons. The cumulative pore volume and the cumulative pore area figures are presented in the Supplementary Information (Figures S8 and S9).

The morphology of the different adsorbents was investigated via SEM (Fig. 7). The activated carbons appear irregular and fractured. In general, they present a lot of similarities, yet the texture of AC-87 is found to be smoother compared to AC-01 and AC-84. FTIR was also applied to analyze the activated carbons before and after adsorption

Table 6
Summary of the properties[a] of the activated carbons.

Property	AC-01	AC-84	AC-87
S_{BET} (m^2 g^{-1})	1213.80	2164.28	947.28
S_{ext} (m^2 g^{-1})	705.76	1726.32	507.42
S_{micro} (m^2 g^{-1})	508.04	437.95	439.85
V_{tot} (cm^3 g^{-1})	1.03	1.43	0.67
V_{micro} (cm^3 g^{-1})	0.24	0.20	0.21
W_{avg} (Å)	56.45	36.48	51.11
pH (-)	4.02	4.77	11.41
TAC (mol g^{-1})	0.991	0.486	0.000
TBC (mol g^{-1})	0.042	0.266	0.922

[a] S_{BET}: specific surface area, S_{ext}: external surface area, S_{micro}: micropore surface area, V_{tot}: total pore volume, V_{micro}: micropore volume, W_{avg}: average pore width, pH: acidity or potential of hydrogen, TAC: total acidic functional groups, TAB: total basic functional groups.

treatment. The spectra of AC-01 and AC-84 before adsorption show similar absorption peaks, among which the most prominent signals are observed at 1060 and 1560 cm^{-1} (Figure S10). These peaks are related to the stretching of C-O and C=C bonds, respectively, which are absent in the case of AC-87. The latter can be due to a difference in the activation process among the adsorbents or to variations in the source material from which they were initially derived [81,82]. In particular, AC-01 and AC-84 are derived from renewable sources, while AC-87 is fossil-based. Nevertheless, all three adsorbent materials show the highest absorbance at wavenumbers smaller than 700 cm^{-1}, which is indicative for C–C stretching, common in activated carbons [83].

More importantly, however, are the changes in the spectra after the adsorption treatment. For this, the corresponding FRs (i.e., the FRs with S > 0.01 wt% in n-butyl acetate and/or cyclohexene), being HBCD, TBBPA and TPHP, were also analyzed by FTIR as pure solids. A summary of these FTIR results for the best-performing activated carbon, AC-84, is shown in Fig. 8. In case of HBCD adsorption, the activated carbon after treatment exhibits new absorption peaks at 665, 690, 820, 860, 880, 1100, 1440, 1460, 2350, and 2940 cm^{-1}, which are all characteristic of the FTIR spectrum of HBCD. The signal at 665 cm^{-1} is the most notable and can be attributed to C-Br stretching of halo compounds. Many other signals can be ascribed to C-H bending or C-H stretching [84–86]. In case of TBBPA adsorption, new absorption peaks of the activated carbon material after treatment are observed at 705, 730, 780, 870, 1130, 1160, 1240, 1270, 1320, 1400, 1470, 2350, and 3475 cm^{-1}, which in turn are all characteristic of the FTIR spectrum of TBBPA. The most prominent signals are those at 705, 870, 1160, 1400, and 3475 cm^{-1}, which are indicative of C-Br stretching of halo compounds or C=C bending, C-H bending, C-O stretching of tertiary alcohols, O-H bending of alcohols, and O-H stretching of alcohols, respectively [84–86]. Finally, in the case of TPHP adsorption, the activated carbon after treatment shows new absorption peaks at 690, 750, 770, 940, 1000, 1160, 1170, 1290, 1480, and 1590 cm^{-1}, which are all characteristic of the FTIR spectrum of TPHP. Among these, the most pronounced signals are those observed at 770, 940, 1000, 1170, and 1590 cm^{-1}, where 770 and 940 cm^{-1} are associated with C=C bending, 1000 cm^{-1} with P-O-C stretching, 1170 cm^{-1} with C-O stretching, and 1590 cm^{-1} with C=C stretching [84–86]. Collectively, these results confirm the successful adherence of these substances onto the adsorbent material, which will be elaborated in more detail in the discussion on the removal of dissolved FRs.

3.3.2. Removal efficiency of the adsorbents towards dissolved flame retardants

Among the selected FRs, three were found to dissolve relatively well in n-butyl acetate and cyclohexene (i.e., S > 1.0 wt%), namely HBCD, TBBPA, and TPHP (Table 3). As a result, these FRs were individually subjected to an adsorption treatment to evaluate their removal efficiency. The corresponding solutions were analyzed via pyrolysis-GC-MS, for which various calibration curves were established (Figures

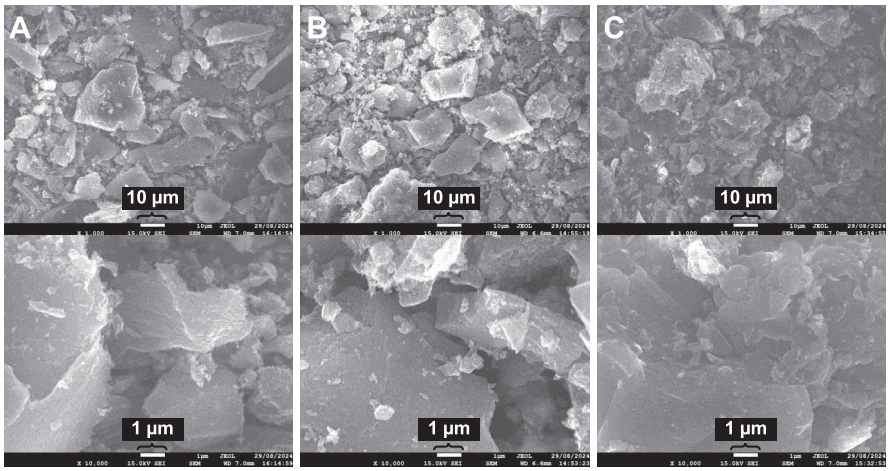

Fig. 7. SEM images of the activated carbons (A) AC-01, (B) AC-84, and (C) AC-87 at magnification 1×10^3 (*top*) and 1×10^4 (*bottom*).

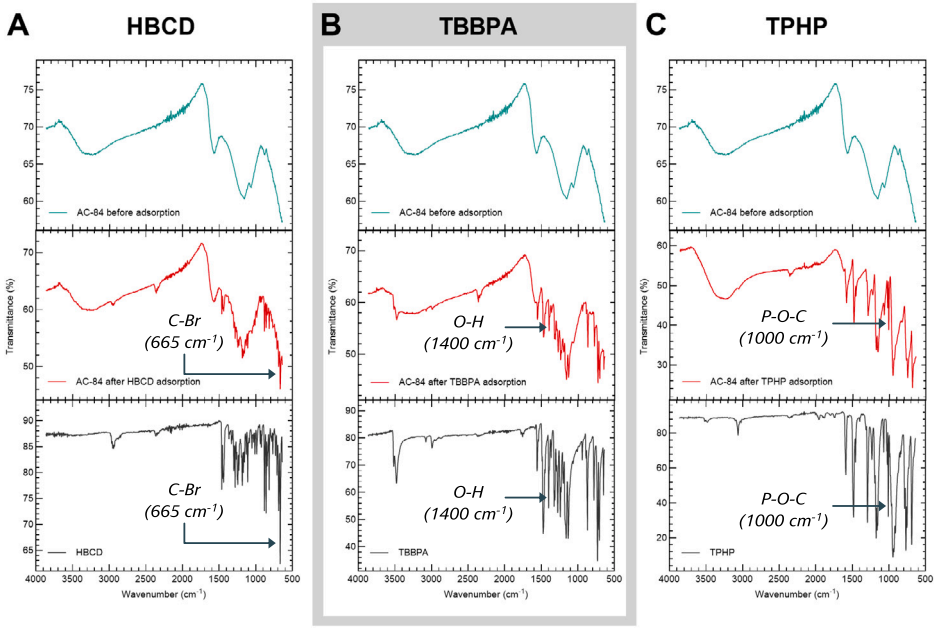

Fig. 8. FTIR spectra of the activated carbon AC-84 before adsorption (*top*), after adsorption (*middle*), and of the flame retardant (*bottom*) for (A) HBCD, (B) TBBPA, and (C) TPHP.

S2–S4). Fig. 9 shows the adsorption results for all n-butyl acetate and cyclohexene mixtures without adding PS. In general, the removal efficiency of the FRs increases with increasing adsorbent dose, which is expected since a higher amount of adsorbent equals a higher amount of available adsorption sites. Typically, such an increase in removal efficiency can be described by a non-linear curve, moving asymptotically towards the theoretical maximum removal efficiency of 100%. Similar behavior is observed in this case, where the increase in removal efficiency is highest in the first half of the curves.

Comparing the solvents, it is apparent that cyclohexene performs significantly better than n-butyl acetate across all mixtures in terms of the FRs' removal efficiency. For instance, at the maximal adsorbent dose of 25 g L^{-1}, HBCD is adsorbed for 95 wt% by AC-84 in cyclohexene, while only for approximately 60 wt% in n-butyl acetate. Similarly, for TBBPA treated with AC-84, a removal efficiency close to 100 wt% is observed in cyclohexene, compared to merely 75 wt% in butyl acetate. For TPHP, this behavior is even more pronounced with a removal efficiency of 80 wt% in cyclohexene and only about 30 wt% in butyl acetate, when treated with AC-84. This trend can be explained by the relatively high affinity of n-butyl acetate for the FRs compared to cyclohexene. The latter is reflected by the solubility of the FRs in these solvents and was also computationally predicted (Table 3). This phenomenon was also observed in earlier work on the removal of a red dye using adsorption in three different organic solvents [59].

Looking at HBCD, the highest removal efficiency of 95 wt% is achieved in cyclohexene when treated with AC-84, whereas AC-01 and AC-87 performed worse with an average decrease in removal efficiency of 12 and 25 wt%, respectively. The difference in adsorbent performance is most pronounced at intermediate adsorbent dose, where the removal efficiency at 10 g L^{-1} for AC-84 is, on average, 27 and 44 wt% higher compared to AC-01 and AC-87, respectively. Similarly, the highest removal efficiency for TBBPA (i.e., 99 wt%) is observed in cyclohexene with AC-84 as the adsorbent. Here, the inferior performance of the other two adsorbent materials results in an average decrease of 17 wt% in removal efficiency. For TPHP, the highest removal efficiency of 80 wt% is also observed in cyclohexene when treated with AC-84, while AC-01 and AC-87 result on average in a 17 and 22 wt% decrease in removal efficiency. Notice that for TPHP, the difference in adsorbent performance when n-butyl acetate is the acting solvent is almost negligible, since the standard deviation of the

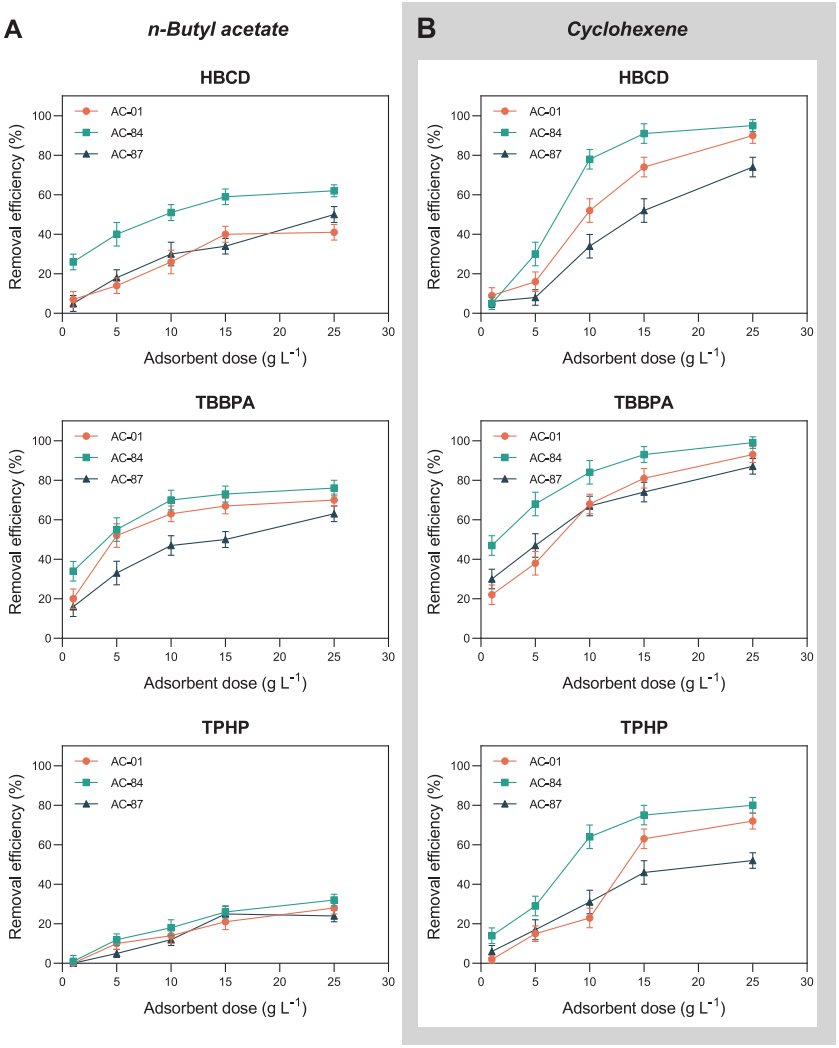

Fig. 9. Adsorption removal efficiency of HBCD (*top*), TBBPA (*middle*), and TPHP (*bottom*) as a function of adsorbent dose by means of activated carbon AC-01 (*orange circles*), AC-84 (*green squares*), and AC-87 (*dark blue triangles*) for solutions of (A) n-butyl acetate and (B) cyclohexene, with a starting concentration of 0.25 wt% at a temperature of 293 ± 1 K.

measurements is similar to the corresponding differences in removal efficiency. This might be due to the relatively low overall removal efficiency of this particular adsorption system (i.e., RE ≤ 32 wt%).

Based on the overall removal efficiencies, it can be derived that the adsorption capacity for TBBPA is similar compared to HBCD, while being significantly higher compared to TPHP. Interestingly, this exact, yet opposite, trend is also observed in their respective solubilities, meaning that the solubility of TPHP in cyclohexene is considerably higher compared to HBCD, which in turn is similar to the solubility of TBBPA. The significant correlation between the adsorption capacity (of the activated carbon) for the dissolved FR and its solubility in the acting solvent, may be driven by the associated difference in intermolecular attraction forces [59]. In other words, a substance with high solubility in a particular solvent, which typically indicates that they share similar physicochemical properties, exhibits a relatively strong intermolecular attraction towards the solvent, rendering physical adsorption to the solid phase (i.e., the adsorbent) more difficult, and vice versa.

Furthermore, AC-84 is overall the most promising type of activated carbon among the evaluated adsorbents, as it consistently yields the highest removal efficiency for all the adsorption systems (Fig. 9). This can be explained by its high specific surface area and total pore volume compared to the other adsorbent materials (Table 6). Moreover, the higher amount of micropores in AC-01 and AC-87 does not seem to have a decisive effect on the removal efficiency of the FRs to compensate for their overall lower specific surface area. However, the calculated lower and upper size limits (i.e., d_{min} and d_{max}, respectively) of the dissolved FRs are generally lower than 2 nm (Table 3), which defines the maximum pore width of the micropores category. Yet, the majority of micropores in activated carbons are typically lower than 1.5 nm [87], while the predicted fraction of all potential orientations of the respective molecules that would fit in a pore with a size ≤ 1.5 nm equals only 33, 20, and 0% for HBCD, TBBPA, and TPHP, respectively. Indeed, the importance of micropores is expected to decrease for the adsorption of larger molecules, such as these FRs [88].

For the best solvent/adsorbent combination, being cyclohexene with AC-84, separate mixtures of the FRs were prepared with the addition of 5 wt% PS. The results are presented in Fig. 10. In general, no significant changes in removal efficiency are observed, meaning that the measurements lie within the range defined by the standard deviation of the prior results (i.e., those without the addition of PS). This indicates that the dissolved PS does not compete with the dissolved FRs for the available adsorption sites, which is, in fact, desired in this context. To validate this, the solutions after adsorption treatment were analyzed via TGA to determine the PS content (Table S7). Since a PS concentration of 5 wt% was recovered, the adsorption capacity of AC-84 for PS seems negligible. Similar results have been described in earlier work [59]. However, the dissolution of PS considerably increases the viscosity of the solution, which may affect the kinetics of the adsorption system.

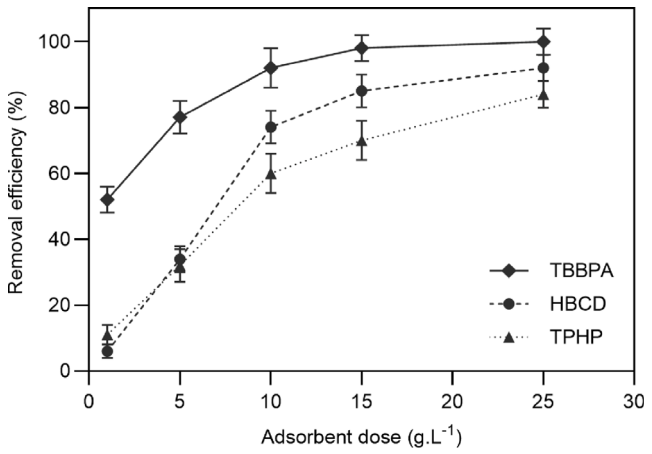

Fig. 10. Adsorption removal efficiency of TBBPA (*solid lines with diamonds*), HBCD (*dashed line with circles*), and TPHP (*dotted line with triangles*) as a function of adsorbent dose by means of activated carbon AC-84 for solutions of cyclohexene with a starting concentration of 0.25 wt% at a temperature of 293 ± 1 K, including 5.0 wt% PS.

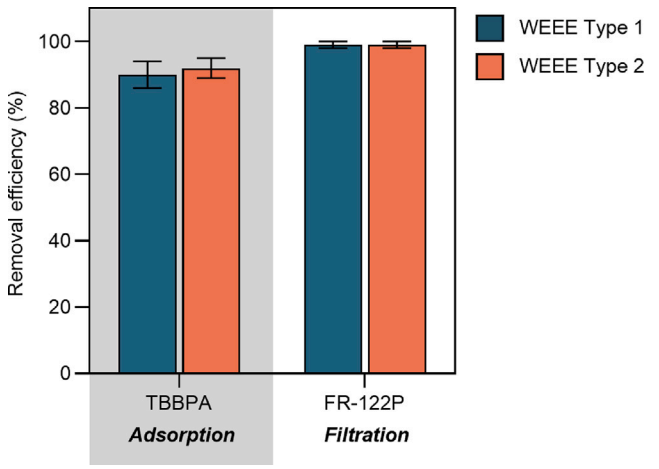

Fig. 11. Removal efficiency of TBBPA by means of adsorption (*left*) and of PolyFR by means of filtration (*right*) for plastic waste samples originating from discarded fridges, i.e., WEEE Type 1 (*dark blue bars*), and for plastic waste samples originating from a mix of smaller electronic devices and household appliances, i.e., WEEE Type 2 (*orange bars*), dissolved in cyclohexene at a concentration of 5.0 wt% and a temperature of 293 ± 1 K.

3.4. Case study: WEEE samples

Analysis of the WEEE samples revealed that both waste streams (i.e., WEEE Type 1 and WEEE Type 2) contained PolyFR and TBBPA. Therefore, the removal efficiency for these two FRs was experimentally determined after subjecting them to the proposed and optimized treatment process. To that end, filtration was performed to target PolyFR after completing dissolution in cyclohexene. Afterward, AC-84 was added to target TBBPA via adsorption. The results are presented in Fig. 11, including both types of WEEE samples. For the filtration part, a near complete removal of PolyFR is observed in both samples (i.e., RE > 99 wt%), which is in line with the expectations considering its near zero solubility in cyclohexene (Table 3) and the results of the filtration experiments discussed earlier (Table 4). For the adsorption part, a removal efficiency of 90 ± 4 wt% and 92 ± 3 wt% is obtained for the waste sample originating from the discarded fridges (WEEE Type 1) and the waste sample originating from the mix of smaller electronic devices and household appliances (WEEE Type 2), respectively. Both results are lower than the previously elaborated adsorption experiments on pure PS solutions spiked with TBBPA, with a removal efficiency of 99 ± 1 wt% at the maximum adsorbent dose of 25 g L^{-1}. This is most likely due to the presence of other dissolved substances in the waste samples, including different FRs next to other additives, such as organic dyes, which may occupy a certain amount of adsorption sites and lower the adsorption capacity of the activated carbon for TBBPA. In addition, differences in the starting concentration of TBBPA may also affect the removal efficiency. Nevertheless, as demonstrated for these two typical WEEE plastic streams, the proposed purification process effectively removes flame retardants, both undissolved and dissolved.

Lastly, it is important to note that for practical implementation in industry, column adsorption is typically the preferred operating approach as opposed to batch adsorption [89]. Column adsorption generally achieves higher removal efficiencies as the adsorbate continuously flows through the adsorbent bed, progressively reducing its concentration in the liquid phase from top to bottom. The concentration gradient between fluid and stationary phase is kept maximum, leading to a higher adsorption rate compared to batch adsorption. Given the relatively high removal efficiencies observed in this study with batch adsorption (i.e., 80 to 99 wt%), it is anticipated that column adsorption could produce an effluent practically free of (halogenated) FRs. This would enable the corresponding dissolution recycling process to yield high-value recyclate, which improves both the material circularity and potentially the profitability of the recycling process. However, to effectively evaluate column adsorption, a comprehensive study of the adsorption kinetics is necessary, including the establishment of breakthrough curves. In particular for polymer solutions, the increased viscosity at industrially relevant polymer concentrations (i.e., 5 to 15 wt%) may reduce the overall mass transfer rate, warranting further research. Additionally, it is worth noting that industrial plants could ultimately target EPS or XPS waste streams, which are rich in brominated flame retardants such as HBCD and are currently not recycled, but rather incinerated or landfilled. Future research should focus on integrating a continuous filtration setup with column adsorption to assess the overall practical feasibility. Moreover, life cycle assessments (LCAs) will be necessary to adequately evaluate the environmental benefits and burdens associated with the new purification method, including the choice of solvent. Lastly, the European Commission's Safe and Sustainable by Design (SSbD) framework is recommended to ensure that such new innovations adhere to sustainable practices and minimize their impact on health, climate, and the environment [90].

4. Conclusion

This study reveals that applying the proposed combination of filtration and adsorption as a purification technique in the dissolution recycling of PS is promising for the removal of FRs. It is demonstrated that FRs with poor solubility in the acting solvent (i.e., S < 0.01 wt%) can be removed successfully via filtration. In contrast, FRs with a higher solubility can be retained effectively via adsorption in a non-aqueous environment. For this, the critical importance of solvent choice is highlighted. It is indicated that the adsorption capacity of activated carbon for the (dissolved) FRs is inversely proportional to the solubility of those FRs in the acting solvent. This study also argues that computational modeling tools like Gaussian16 and COSMO-RS can characterize the target substances, as demonstrated in this work, and ultimately screen different solvents to identify the most optimal purification system. However, careful selection of the models is advised where additionally the required computational power may become extensive, especially for large molecules (i.e., M > 800 g mol^{-1}) or when multiple conformers are required to adequately describe the molecule's behavior. With respect to the type of activated carbon, it appears that the adsorption of the FRs does not benefit significantly from the presence of micropores. Furthermore, next to the analysis on the removal of five different FRs (i.e., HBCD, TBBPA, DBDPE, TPHP,

and PolyFR) in a controlled environment from virgin PS mixtures, also two types of plastic WEEE fractions were included. It was demonstrated that FRs can still be removed based on filtration and adsorption, with slightly reduced efficiencies in the adsorption step, probably caused by competition. In conclusion, implementing adsorption (in combination with filtration) in the context of dissolution or solvent-based recycling of plastics seems promising to primarily target problematic additives and contaminants currently impeding plastic recycling rates. Future work on optimizing the recovery of the polymer from the purified organic solution is recommended to facilitate the recycling process further and aim for true plastic circularity.

CRediT authorship contribution statement

Michiel Van Melkebeke: Writing – original draft, Visualization, Software, Methodology, Investigation, Conceptualization. **Rita Kol:** Methodology, Investigation. **Amin Shariatmadar Tehrani:** Visualization, Software, Methodology, Investigation. **Dave Manhaeghe:** Investigation. **Emile Casiries:** Investigation. **Tine Van Laere:** Investigation. **Yufei Xie:** Investigation. **Hamed Mohamadzadeh Shirazi:** Investigation. **Norbert Niessner:** Writing – review & editing. **Dirk Reichert:** Writing – review & editing. **Hilde Poelman:** Writing – review & editing. **Kevin Van Geem:** Writing – review & editing. **Steven De Meester:** Writing – review & editing, Supervision, Resources, Project administration, Methodology, Funding acquisition, Conceptualization.

Declaration of competing interest

The authors declare that they have no known competing financial interests or personal relationships that could have appeared to influence the work reported in this paper.

Acknowledgments

The authors thank DESOTEC, INEOS Styrolution, and Neue Materialien Bayreuth GmbH for their kind cooperation and for providing the necessary materials. This work was performed in the framework of the Moonshot cluster SBO project PREFER (HBC.2020.2609 "The plastics refinery: no more waste"), with the financial support of VLAIO (Flemish Agency for Innovation and Entrepreneurship) via the Flemish spearhead cluster Catalisti. In addition, the authors would like to express their gratitude towards INEOS Styrolution for the financial support provided for this research, which is part of the project CIRCULARS which is also publicly funded by VLAIO. Lastly, this work was partially performed within the framework of the Renovate 2 project as well.

Appendix A. Supplementary data

Supplementary material related to this article can be found online at https://doi.org/10.1016/j.cej.2025.164504.

Data availability

Data will be made available on request.

References

[1] R.C. Thompson, S.H. Swan, C.J. Moore, F.S.V. Saal, Our plastic age, Phil. Trans. R. Soc. B 364 (2009) 1973–1976, http://dx.doi.org/10.1098/rstb.2009.0054.
[2] A.L. Andrady, M.A. Neal, Applications and societal benefits of plastics, Phil. Trans. R. Soc. B 364 (2009) 1977–1984, http://dx.doi.org/10.1098/rstb.2008.0304.
[3] J. Boucher, G. Billard, E. Simeone, J. Sousa, The marine plastic footprint: Towards a science-based metric for measuring marine plastic leakage and increasing the materiality and circularity of plastic, 2020, http://dx.doi.org/10.2305/IUCN.CH.2020.01.en.
[4] L. Cabernard, S. Pfister, C. Oberschelp, S. Hellweg, Growing environmental footprint of plastics driven by coal combustion, Nat. Sustain. 5 (2022) 139–148, http://dx.doi.org/10.1038/s41893-021-00807-2.
[5] D. Lithner, A. Larsson, G. Dave, Environmental and health hazard ranking and assessment of plastic polymers based on chemical composition, Sci. Total Environ. 409 (2011) 3309–3324, http://dx.doi.org/10.1016/j.scitotenv.2011.04.038.
[6] L. Hermabessiere, A. Dehaut, I. Paul-Pont, C. Lacroix, R. Jezequel, P. Soudant, G. Duflos, Occurrence and effects of plastic additives on marine environments and organisms: A review, Chemosphere 182 (2017) 781–793, http://dx.doi.org/10.1016/j.chemosphere.2017.05.096.
[7] R. Geyer, J.R. Jambeck, K.L. Law, Production, use, and fate of all plastics ever made, 2017, URL https://www.science.org/doi/10.1126/sciadv.1700782.
[8] Y. Chen, A.K. Awasthi, F. Wei, Q. Tan, J. Li, Single-use plastics: Production, usage, disposal, and adverse impacts, Sci. Total Environ. 752 (2021) http://dx.doi.org/10.1016/j.scitotenv.2020.141772.
[9] I.E. Napper, R.C. Thompson, Plastic debris in the marine environment: History and future challenges, Glob. Challenges 4 (2020) http://dx.doi.org/10.1002/gch2.201900081.
[10] R. Kumar, A. Verma, A. Shome, R. Sinha, S. Sinha, P.K. Jha, R. Kumar, P. Kumar, Shubham, S. Das, P. Sharma, P.V. Prasad, Impacts of plastic pollution on ecosystem services, sustainable development goals, and need to focus on circular economy and policy interventions, Sustain. (Switzerland) 13 (2021) http://dx.doi.org/10.3390/su13179963.
[11] E. Palm, J. Hasselbalch, K. Holmberg, T.D. Nielsen, Narrating plastics governance: policy narratives in the European plastics strategy, Environ. Politics 31 (2022) 365–385, http://dx.doi.org/10.1080/09644016.2021.1915020.
[12] C. Jehanno, J.W. Alty, M. Roosen, S.D. Meester, A.P. Dove, E.Y. Chen, F.A. Leibfarth, H. Sardon, Critical advances and future opportunities in upcycling commodity polymers, Nature 603 (2022) 803–814, http://dx.doi.org/10.1038/s41586-021-04350-0.
[13] Plastics Europe, Plastics: the fast facts 2023, 2023.
[14] Plastics Europe, The circular economy for plastics executive summary, 2024.
[15] P. Billen, S.D. Meester, Editorial overview: Toward cruising speed for circular plastics, Curr. Opin. Green Sustain. Chem. 44 (2023) http://dx.doi.org/10.1016/j.cogsc.2023.100872.
[16] J.G. Rosenboom, R. Langer, G. Traverso, Bioplastics for a circular economy, Nat. Rev. Mater. 7 (2022) 117–137, http://dx.doi.org/10.1038/s41578-021-00407-8.
[17] K. Ragaert, L. Delva, K.V. Geem, Mechanical and chemical recycling of solid plastic waste, Waste Manage. 69 (2017) 24–58, http://dx.doi.org/10.1016/J.WASMAN.2017.07.044.
[18] J.P. Lange, S.R. Kersten, S.D. Meester, M.C. van Eijk, K. Ragaert, Plastic recycling stripped naked – from circular product to circular industry with recycling cascade, ChemSusChem (2024) http://dx.doi.org/10.1002/cssc.202301320.
[19] I. Vollmer, M.J. Jenks, M.C. Roelands, R.J. White, T. van Harmelen, P. de Wild, G.P. van der Laan, F. Meirer, J.T. Keurentjes, B.M. Weckhuysen, Beyond mechanical recycling: Giving new life to plastic waste, Angew. Chem. - Int. Ed. 59 (2020) 15402–15423, http://dx.doi.org/10.1002/anie.201915651.
[20] D. Damayanti, D.R. Saputri, D.S.S. Marpaung, F. Yusupandi, A. Sanjaya, Y.M. Simbolon, W. Asmarani, M. Ulfa, H.S. Wu, Current prospects for plastic waste treatment, Polymers 14 (2022) http://dx.doi.org/10.3390/polym14153133.
[21] K. Ragaert, C. Ragot, K.M.V. Geem, S. Kersten, Y. Shiran, S.D. Meester, Clarifying European terminology in plastics recycling, Curr. Opin. Green Sustain. Chem. 44 (2023) http://dx.doi.org/10.1016/j.cogsc.2023.100871.
[22] S. Chen, Y.H. Hu, Advancements and future directions in waste plastics recycling: From mechanical methods to innovative chemical processes, Chem. Eng. J. 493 (2024) http://dx.doi.org/10.1016/j.cej.2024.152727.
[23] M. Kusenberg, M. Roosen, A. Doktor, L. Casado, A.J. Abdulrahman, B. Parvizi, A. Eschenbacher, E. Biadi, N. Laudou, D. Jänsch, S.D. Meester, K.M.V. Geem, Contaminant removal from plastic waste pyrolysis oil via depth filtration and the impact on chemical recycling: A simple solution with significant impact, Chem. Eng. J. 473 (2023) http://dx.doi.org/10.1016/j.cej.2023.145259.
[24] X. Zhao, M. Korey, K. Li, K. Copenhaver, H. Tekinalp, S. Celik, K. Kalaitzidou, R. Ruan, A.J. Ragauskas, S. Ozcan, Plastic waste upcycling toward a circular economy, Chem. Eng. J. 428 (2022) http://dx.doi.org/10.1016/j.cej.2021.131928.
[25] Q. Liu, S. Martinez-Villarreal, S. Wang, N.N.T. Tien, M. Kammoun, Q.D. Roover, C. Len, A. Richel, The role of plastic chemical recycling processes in a circular economy context, Chem. Eng. J. 498 (2024) http://dx.doi.org/10.1016/j.cej.2024.155227.
[26] T. Rieger, J.C. Oey, V. Palchyk, A. Hofmann, M. Franke, A. Hornung, Chemical recycling of WEEE plastics—production of high purity monocyclic aromatic chemicals, Processes 9 (2021) http://dx.doi.org/10.3390/pr9030530.
[27] M.A. Charitopoulou, K.G. Kalogiannis, A.A. Lappas, D.S. Achilias, Novel trends in the thermo-chemical recycling of plastics from WEEE containing brominated flame retardants, Environ. Sci. Pollut. Res. (2021) http://dx.doi.org/10.1007/s11356-020-09932-5.
[28] R. Wang, Z. Xu, Recycling of non-metallic fractions from waste electrical and electronic equipment (WEEE): A review, Waste Manage. 34 (2014) 1455–1469, http://dx.doi.org/10.1016/j.wasman.2014.03.004.

[29] M. Bientinesi, L. Petarca, Comparative environmental analysis of waste brominated plastic thermal treatments, Waste Manage. 29 (2009) 1095–1102, http://dx.doi.org/10.1016/j.wasman.2008.08.004.
[30] M.A. Charitopoulou, L. Papadopoulou, D.S. Achilias, Effect of brominated flame retardant on the pyrolysis products of polymers originating in WEEE, Environ. Sci. Pollut. Res. (2022) http://dx.doi.org/10.1007/s11356-021-15489-8.
[31] M. Solis, S. Silveira, Technologies for chemical recycling of household plastics – a technical review and TRL assessment, Waste Manage. 105 (2020) 128–138, http://dx.doi.org/10.1016/J.WASMAN.2020.01.038.
[32] P.R. Jadhao, E. Ahmad, K.K. Pant, K.D.P. Nigam, Advancements in the field of electronic waste recycling: Critical assessment of chemical route for generation of energy and valuable products coupled with metal recovery, Sep. Purif. Technol. 289 (2022) 120773, http://dx.doi.org/10.1016/j.seppur.2022.120773.
[33] P. Das, Q. Zeng, A. Leybros, J.C.P. Gabriel, C.Y. Tay, J.M. Lee, Enhanced extraction of brominated flame retardants from e-waste plastics, Chem. Eng. J. 469 (2023) http://dx.doi.org/10.1016/j.cej.2023.144126.
[34] Y. Wan, Q. Zeng, P. Shi, Y.J. Yoon, C.Y. Tay, J.M. Lee, Machine learning-assisted optimization of TBBPA-bis-(2,3-dibromopropyl ether) extraction process from ABS polymer, Chemosphere 287 (2022) http://dx.doi.org/10.1016/j.chemosphere.2021.132128.
[35] D. Xia, A. Maurice, A. Leybros, J.M. Lee, A. Grandjean, J.C.P. Gabriel, On-line spectroscopic study of brominated flame retardant extraction in supercritical CO2, Chemosphere 263 (2021) http://dx.doi.org/10.1016/j.chemosphere.2020.128282.
[36] Y. Wan, Q. Zeng, I. Kim, P. Shi, Y.J. Yoon, C.Y. Tay, J.M. Lee, Ultrasonic-assisted tetrabromobisphenol A-bis-(2,3-dibromo-2-methylpropyl ether) extraction process from ABS polymer supported by machine learning, Environ. Technol. Innov. 27 (2022) http://dx.doi.org/10.1016/j.eti.2022.102485.
[37] M. Roosen, L. Harinck, S. Ügdüler, T.D. Somer, A.G. Hucks, T.G. Belé, A. Buettner, K. Ragaert, K.M.V. Geem, A. Dumoulin, S.D. Meester, Deodorization of post-consumer plastic waste fractions: A comparison of different washing media, Sci. Total Environ. 812 (2022) http://dx.doi.org/10.1016/j.scitotenv.2021.152467.
[38] S. Ügdüler, T.D. Somer, K.M.V. Geem, M. Roosen, A. Kulawig, R. Leineweber, S.D. Meester, Towards a better understanding of delamination of multilayer flexible packaging films by carboxylic acids, ChemSusChem 14 (2021) 4198–4213, http://dx.doi.org/10.1002/cssc.202002877.
[39] J.C.J. Bart, Additives in Polymers: Industrial Analysis and Applications, Wiley, 2005, pp. 803–819, http://dx.doi.org/10.1002/0470012064.
[40] L. Anderson, E. Yu, W.T. Chen, Chemical recycling of mixed plastics in electronic waste using solvent-based processing, Processes 10 (2022) http://dx.doi.org/10.3390/pr10010066.
[41] C. Chaine, A.S. Hursthouse, B. McLean, I. McLellan, B. McMahon, J. McNulty, J. Miller, E. Viza, Recycling plastics from WEEE: A review of the environmental and human health challenges associated with brominated flame retardants, Int. J. Environ. Res. Public Heal. 19 (2022) http://dx.doi.org/10.3390/ijerph19020766.
[42] M. Alaee, P. Arias, A. Sjödin, Å. Bergman, An overview of commercially used brominated flame retardants, their applications, their use patterns in different countries/regions and possible modes of release, Environ. Int. 29 (2003) 683–689, http://dx.doi.org/10.1016/S0160-4120(03)00121-1.
[43] P. Hennebert, Concentrations of brominated flame retardants in plastics of electrical and electronic equipment, vehicles, construction, textiles and non-food packaging: A review of occurrence and management, Detritus 12 (2020) 34–50, http://dx.doi.org/10.31025/2611-4135/2020.13997.
[44] M. Roosen, N. Mys, M. Kusenberg, P. Billen, A. Dumoulin, J. Dewulf, K.M.V. Geem, K. Ragaert, S.D. Meester, Detailed analysis of the composition of selected plastic packaging waste products and its implications for mechanical and thermochemical recycling, Environ. Sci. Technol. 54 (2020) 13282–13293, http://dx.doi.org/10.1021/acs.est.0c03371.
[45] A. Chagnes, C. Ekberg, T. Retegan, G. Cote, M. Nilsson, WEEE Recycling: Research, Development, and Policies, Elsevier, 2017, http://dx.doi.org/10.1016/C2014-0-03743-4.
[46] J. Lee, H. Choi, J. Kim, Environmental and economic impacts of e-waste recycling: A systematic review, Chem. Eng. J. 494 (2024) http://dx.doi.org/10.1016/j.cej.2024.152917.
[47] J.N. Hahladakis, C.A. Velis, R. Weber, E. Iacovidou, P. Purnell, An overview of chemical additives present in plastics: Migration, release, fate and environmental impact during their use, disposal and recycling, J. Hazard. Mater. 344 (2018) 179–199, http://dx.doi.org/10.1016/j.jhazmat.2017.10.014.
[48] S.J. Chen, Y.J. Ma, J. Wang, D. Chen, X.J. Luo, B.X. Mai, Brominated flame retardants in children's toys: Concentration, composition, and children's exposure and risk assessment, Environ. Sci. Technol. 43 (2009) 4200–4206, http://dx.doi.org/10.1021/es9004834.
[49] A.C. Ionas, A.C. Dirtu, T. Anthonissen, H. Neels, A. Covaci, Downsides of the recycling process: Harmful organic chemicals in children's toys, Environ. Int. 65 (2014) 54–62, http://dx.doi.org/10.1016/j.envint.2013.12.019.
[50] M.M. Dingemans, M. van den Berg, R.H. Westerink, Neurotoxicity of brominated flame retardants: (in)direct effects of parent and hydroxylated polybrominated diphenyl ethers on the (developing) nervous system, Environ. Health Perspect. 119 (2011) 900–907, http://dx.doi.org/10.1289/ehp.1003035.
[51] S.H. Brandsma, P.E. Leonards, J.C. Koekkoek, J. Samsonek, F. Puype, Migration of hazardous contaminants from WEEE contaminated polymeric toy material by mouthing, Chemosphere 294 (2022) http://dx.doi.org/10.1016/j.chemosphere.2022.133774.
[52] J.L. Lyche, C. Rosseland, G. Berge, A. Polder, Human health risk associated with brominated flame-retardants (BFRs), Environ. Int. 74 (2015) 170–180, http://dx.doi.org/10.1016/j.envint.2014.09.006.
[53] H.S. Hendriks, R.H. Westerink, Neurotoxicity and risk assessment of brominated and alternative flame retardants, Neurotoxicol. Teratol. 52 (2015) 248–269, http://dx.doi.org/10.1016/j.ntt.2015.09.002.
[54] A. Guzzonato, F. Puype, S.J. Harrad, Evidence of bad recycling practices: BFRs in children's toys and food-contact articles, Environ. Sci.: Process. Impacts 19 (2017) 956–963, http://dx.doi.org/10.1039/c7em00160f.
[55] M.W. Beach, D.A. Beaudoin, I. Beulich, J.C. Bloom, J.W. Davis, H.M. Hollnagel, J.W. Hull, B. King, S. Kram, C. Lukas, M. Matteucci, T. Morgan, B. Stobby, New class of brominated polymeric flame retardants for use in polystyrene foams, Cell. Polym. 32 (2013) http://dx.doi.org/10.1177/026248931303200403.
[56] P. Fjäder, T. Turunen, P. Rinne, E. Häkkinen, S. Kauppi, T. Sormunen, M. Andersson, Harmful additives in WEEE plastics and the regulatory framework, 2022.
[57] P. Xiong, X. Yan, Q. Zhu, G. Qu, J. Shi, C. Liao, G. Jiang, A review of environmental occurrence, fate, and toxicity of novel brominated flame retardants, Environ. Sci. Technol. 53 (2019) 13551–13569, http://dx.doi.org/10.1021/acs.est.9b03159.
[58] R. Wang, H. Cheng, Y. Gong, T. Huang, New brominated flame retardant decabromodiphenyl ethane (DBDPE) in water sediments: A review of contamination characteristics, exposure pathways, ecotoxicological effects and health risks, Environ. Pollut. 334 (2023) http://dx.doi.org/10.1016/j.envpol.2023.122121.
[59] M. Van Melkebeke, T.D. Somer, T.V. Laere, T.N.L. Minh, H.M. Shirazi, H. Poelman, K.V. Geem, S.D. Meester, Adsorption modeling for contaminant removal in plastic dissolution recycling: Investigating an amino ketone-based red dye, Sep. Purif. Technol. 331 (2024) http://dx.doi.org/10.1016/j.seppur.2023.125559.
[60] R. Kol, R. Denolf, G. Bernaert, D. Manhaeghe, E. Bar-Ziv, G.W. Huber, N. Niessner, M. Verswyvel, A. Lemonidou, D.S. Achilias, S.D. Meester, Increasing the dissolution rate of polystyrene waste in solvent-based recycling, ACS Sustain. Chem. Eng. 12 (2024) 4619–4630, http://dx.doi.org/10.1021/acssuschemeng.3c08154.
[61] S. Brunauer, P.H. Emmett, E. Teller, Adsorption of gases in multimolecular layers, J. Am. Chem. Soc. 60 (1938) 309–319, http://dx.doi.org/10.1021/ja01269a023.
[62] B.C. Lippens, B.G. Linsen, J. Boer, Studies on pore systems in catalysts I. The adsorption of nitrogen; apparatus and calculation, J. Catalysis 3 (1964) 32–37, http://dx.doi.org/10.1016/0021-9517(64)90089-2.
[63] E.P. Barrett, L.G. Joyner, P.P. Halenda, The determination of pore volume and area distributions in porous substances. I. Computations from nitrogen isotherms, J. Am. Chem. Soc. 73 (1951) 373–380, http://dx.doi.org/10.1021/ja01145a126, doi: 10.1021/ja01145a126.
[64] M.J. Frisch, G.W. Trucks, H.B. Schlegel, G.E. Scuseria, M.A. Robb, J.R. Cheeseman, G. Scalmani, V. Barone, G.A. Petersson, H. Nakatsuji, X. Li, M. Caricato, A.V. Marenich, J. Bloino, B.G. Janesko, R. Gomperts, B. Mennucci, H.P. Hratchian, J.V. Ortiz, A.F. Izmaylov, J.L. Sonnenberg, D. Williams-Young, F. Ding, F. Lipparini, F. Egidi, J. Goings, B. Peng, A. Petrone, T. Henderson, D. Ranasinghe, V.G. Zakrzewski, J. Gao, N. Rega, G. Zheng, W. Liang, M. Hada, M. Ehara, K. Toyota, R. Fukuda, J. Hasegawa, M. Ishida, T. Nakajima, Y. Honda, O. Kitao, H. Nakai, T. Vreven, K. Throssell, J.A.M. Jr., J.E. Peralta, F. Ogliaro, M.J. Bearpark, J.J. Heyd, E.N. Brothers, K.N. Kudin, V.N. Staroverov, T.A. Keith, R. Kobayashi, J. Normand, K. Raghavachari, A.P. Rendell, J.C. Burant, S.S. Iyengar, J. Tomasi, M. Cossi, J.M. Millam, M. Klene, C. Adamo, R. Cammi, J.W. Ochterski, R.L. Martin, K. Morokuma, O. Farkas, J.B. Foresman, D.J. Fox, Gaussian16 Revision C.01, Gaussian Inc., Wallingford CT, 2016.
[65] Cheminformatics Software, RDKit: Open-Source, URL https://www.rdkit.org/.
[66] A. Klamt, F. Eckert, W. Arlt, COSMO-RS: An alternative to simulation for calculating thermodynamic properties of liquid mixtures, Annu. Rev. Chem. Biomol. Eng. 1 (2010) 101–122, http://dx.doi.org/10.1146/annurev-chembioeng-073009-100903.
[67] A.D. Becke, Density-functional thermochemistry. III. The role of exact exchange, J. Chem. Phys. 98 (1993) 5648–5652, http://dx.doi.org/10.1063/1.464913.
[68] C. Lee, Y. eitao, R.G. Parr, Development of the Colic-Salvetti correlation-energy formula into a functional of the electron density, Phys Rev B Condens. Matter 37 (1988) 15–1988, http://dx.doi.org/10.1103/physrevb.37.785.
[69] S. Grimme, J. Antony, S. Ehrlich, H. Krieg, A consistent and accurate ab initio parametrization of density functional dispersion correction (DFT-d) for the 94 elements H-pu, J. Chem. Phys. 132 (2010) http://dx.doi.org/10.1063/1.3382344.
[70] Dassault Systèmes, BIOVIA cosmotherm, 2020.
[71] R. Kol, E. Carrieri, S. Gusev, M. Verswyvel, N. Niessner, A. Lemonidou, D.S. Achilias, S.D. Meester, Removal of undissolved substances in the dissolution-based recycling of polystyrene waste by applying filtration and centrifugation, Sep. Purif. Technol. 325 (2023) http://dx.doi.org/10.1016/j.seppur.2023.124682.

[72] L. Hou, Z. Wang, P. Song, A precise combined complete blocking and cake filtration model for describing the flux variation in membrane filtration process with BSA solution, J. Membr. Sci. 542 (2017) 186–194, http://dx.doi.org/10.1016/j.memsci.2017.08.013.

[73] J. Hermia, Constant pressure blocking filtration laws - application to power-law non-newtonian fluids, Trans. Inst. Chem. Eng. (1982) URL https://api.semanticscholar.org/CorpusID:61145250.

[74] M.C.V. Vela, S.Á. Blanco, J.L. García, E.B. Rodríguez, Analysis of membrane pore blocking models applied to the ultrafiltration of PEG, Sep. Purif. Technol. 62 (2008) 489–498, http://dx.doi.org/10.1016/j.seppur.2008.02.028.

[75] K. Soetaert, T. Petzoldt, Inverse modelling, sensitivity and Monte Carlo analysis in R using package FME, J. Stat. Softw. 33 (2010) http://dx.doi.org/10.18637/jss.v033.i03.

[76] S. Heidari, H. Etemadi, R. Yegani, A comprehensive analysis of membrane fouling in microfiltration of complex linear macromolecules based on theoretical modeling and FESEM images, J. Chem. Technol. Biotechnol. 96 (2021) 360–373, http://dx.doi.org/10.1002/jctb.6548.

[77] R.W. Gerlach, D.E. Dobb, G.A. Raab, J.M. Nocerino, Gy sampling theory in environmental studies. 1. Assessing soil splitting protocols, J. Chemom. 16 (2002) 321–328, http://dx.doi.org/10.1002/cem.705.

[78] G.M. Silva, D.A. Pantano, S. Loehlé, J.A. Coutinho, The challenges of using COSMO-RS to describe polymer solution behavior, Ind. Eng. Chem. Res. 62 (2023) 20936–20944, http://dx.doi.org/10.1021/acs.iecr.3c03310.

[79] M.W. Beach, K.L. Kearns, J.W. Davis, J.R. Stutzman, D. Lee, Y. Lai, D. Monaenkova, S. Kram, J. Hu, C. Lukas, Stability assessment of a polymeric brominated flame retardant in polystyrene foams under application-relevant conditions, Environ. Sci. Technol. 55 (2021) 3050–3058, http://dx.doi.org/10.1021/acs.est.0c04325.

[80] E. Zurob, R. Cabezas, E. Villarroel, N. Rosas, G. Merlet, E. Quijada-Maldonado, J. Romero, A. Plaza, Design of natural deep eutectic solvents for the ultrasound-assisted extraction of hydroxytyrosol from olive leaves supported by COSMO-RS, Sep. Purif. Technol. 248 (2020) http://dx.doi.org/10.1016/j.seppur.2020.117054.

[81] S.K. Shahcheragh, M.M.B. Mohagheghi, A. Shirpay, Effect of physical and chemical activation methods on the structure, optical absorbance, band gap and urbach energy of porous activated carbon, SN Appl. Sci. 5 (2023) http://dx.doi.org/10.1007/s42452-023-05559-6.

[82] R. Ali, Z. Aslam, R.A. Shawabkeh, A. Asghar, I.A. Hussein, BET, FTIR, and RAMAN characterizations of activated carbon from waste oil fly ash, Turk. J. Chem. 44 (2020) 279–295, http://dx.doi.org/10.3906/KIM-1909-20.

[83] A.I. Bakti, P.L. Gareso, Characterization of active carbon prepared from coconuts shells using FTIR, XRD and SEM techniques, J. Ilm. Pendidik. Fis. Al- Biruni 7 (2018) 33–39, http://dx.doi.org/10.24042/jipfalbiruni.v7i1.2459.

[84] B. Smith, Infrared Spectral Interpretation: A Systematic Approach, first ed., CRC Press, 1998.

[85] J. Coates, Interpretation of infrared spectra, a practical approach, Encycl. Anal. Chem. (2000) 10815–10837.

[86] LibreTexts, Infrared Spectroscopy Absorption Table, URL https://chem.libretexts.org/Ancillary_Materials/Reference/Reference_Tables/Spectroscopic_Reference_Tables/Infrared_Spectroscopy_Absorption_Table.

[87] A.A. Shiryaev, P. Pré, C. Pardanaud, V. Murzin, A. Averin, J.N. Rouzaud, Microporosity and nanostructure of activated carbons: characterization by X-ray diffraction and scattering, Raman spectroscopy and transmission electron microscopy, Adsorption 29 (2023) 275–289, http://dx.doi.org/10.1007/s10450-023-00406-x.

[88] O.-W. Achaw, in: V. Kazmiruk (Ed.), A Study of the Porosity of Activated Carbons Using the Scanning Electron Microscope, IntechOpen, Rijeka, 2012, http://dx.doi.org/10.5772/36337.

[89] H. Patel, Comparison of batch and fixed bed column adsorption: a critical review, Int. J. Environ. Sci. Technol. (2021) http://dx.doi.org/10.1007/s13762-021-03492-y.

[90] European Commission, Commission recommendation (EU) 2022/2510 of 8 december 2022: establishing a European assessment framework for ‘safe and sustainable by design’ chemicals and materials, 2022.